


Dynamic instabilities under isotropic drained compression of idealized granular materials

T. Doanh¹  · N. Abdelmoula¹ · L. Gribaa¹ · T. T. T. Nguyễn¹ · S. Hans¹ · C. Boutin¹ · A. Le Bot²

Received: 11 May 2016 / Accepted: 1 December 2016 / Published online: 27 December 2016
© Springer-Verlag Berlin Heidelberg 2016

Abstract The compressibility behaviour of loose and contracting granular assemblies, normally consolidated and overconsolidated, under isotropic drained compression is investigated in this paper. Short cylindrical samples of water-saturated monodisperse glass beads, initially assembled in loose state by moist-tamping technique, are isotropically compressed in a classical axisymmetric triaxial machine. Very loose glass bead samples experience numerous unexpected events, sometimes cascading, under undetermined triggered effective isotropic stress in loading and in unloading, while the classical compressibility behaviour of granular material is recovered once these events ignored. Each event, resembling the stick–slip instability during shear in triaxial compression, is characterized by a transient dynamic phase I with very fast drop of effective isotropic stress σ' due to an excess pore pressure development at nearly constant volume and constant axial strain, followed by a quasi-static phase II with gradual increase in axial ε_a (contraction) and volumetric ε_v (compaction) strain, and a full progressive recovery of σ' to the previous level before event. A short-lived liquefaction with null σ' measured in the first phase I results in a local collapse state. Collapse events also happen on unsaturated moist and dry states. Rare events even occur during the

unloading of subsequent isotropic compression cycles. The effects of triggered isotropic stress are discussed, the instability characteristics measured, the comparison with stick–slip instability made and the hypothesis of micro-structural instability with local collapse of contact networks and rapid micro-structural rearrangement argued.

Keywords Collapse · Dynamic · Friction · Idealized granular materials · Instability · Isotropic consolidation

1 Introduction

In granular mechanics, a large number of intensive theoretical and experimental studies have been devoted to the understanding of the mechanical behaviour of granular materials. Despite this large body of knowledge, many aspects such as inherent and induced anisotropy, principal stress rotation, cyclic loading and liquefaction still remain puzzling subjects for granular scientists [76]. Even today, these sophisticated rheological features are not well simulated by recent constitutive relations, due to the increasing complexity revealed by experiments, and also often due to the phenomenological-based character of these relations inside the continuous mechanics framework [29].

One of the key ideas to overcome the complexity of real granular media is to test in the laboratory some simplified and idealized granular materials consisting of perfectly rounded particles. Although monodisperse glass beads certainly cannot be representative of real natural granular materials consisting of mostly non-spherical particles like sand, it can constitute a useful comprehensive laboratory first step towards a better understanding of the latter.

The second key idea is to take advantage of recent advances of powerful computing and imaging techniques,

Electronic supplementary material The online version of this article (doi:10.1007/s11440-016-0514-0) contains supplementary material, which is available to authorized users.

✉ T. Doanh
thiep.doanh@entpe.fr

¹ Ecole Nationale des Travaux Publics de l'Etat, LGCB, LTDS (UMR 5513), 2 Rue M. Audin, 69518 Vaulx en Velin Cedex, France

² Ecole Centrale de Lyon, LTDS (UMR 5513), 36 avenue Guy-de-Collongue, 69134 Ecully Cedex, France

delicate mechanical investigation in the laboratory might be replaced by numerical simulation of a large collection of particles using discrete element method (DEM [51, 57]) pioneered by Cundall and Strack [11] and popularized by Thornton [68]. One of the objectives was to derive the macroscopic behaviour using only the microscopic parameters of individual particles. Many salient features of granular media are qualitatively retrieved [43, 44, 56, 62], although quantitative comparisons [52, 65] are rare. The coordination number, the distribution of contact orientations are rapidly identified as relevant parameters. These variables are usually unattainable in real experiments, even for recent computer tomography (CT) investigations.

However, spherical particles can slide, slip and roll with respect to each other, contrasting the grain to grain interlocking capability due to the angular shape of most natural sand grains. Packings of rounded particles create unexpected experimental behaviour, known as stick–slip phenomenon, similar to earthquakes with very fast period of stress release over long period of strain accumulation.

Experimental physicists began to investigate first the behaviour of thin layers of a few tens of mono-sized spherical grains subjected to shear forces in specially designed slider frictional machine similar to the simple shear apparatus in soil mechanics. The main objective was to study the frictional mechanisms at fundamental level [55]. The vertical and horizontal motions of a light cover on top of thin particle layers were measured. The light cover, pushed by a calibrated spring, imposes very low normal stress. Stick–slips occur for horizontal motion and the main controlling factors were rapidly identified and their effects evaluated: the low driving velocity, the stiffness of the spring system and the normal force. As in simple shear technique, the vertical displacement was taken as a representative measure for the dilatancy characteristics of the granular media, providing a constant cross section [26, 48].

Model granular materials in thin layers are also used as a substitute of gouge materials in fault zones in rock mechanics [6, 41, 42]; and the observed one-dimensional stick–slip often tentatively explained by “rate and state” constitutive equations [14, 42, 61], usually associated with contact ageing [32] and velocity dependency of frictional behaviour [32, 42].

The annular shear cell developed for soil mechanics was used next by physicists to study the behaviour of glass beads under unlimited large strains and constant normal stress [10, 67], leading to a significant role of volumetric strain on stick–slip phenomenon. Quasi regular stick–slips were observed and large volumetric contraction (respt. dilation) was measured during the slip (respt. stick) phase. Small amount of creep was also detected before and after slip event, as in [48]. Periodic dilatancy and contractancy was proposed as the origin of stick–slip instabilities.

However, the precise triggering mechanisms were still missing. As noted above, noisy volumetric strain was derived only from vertical displacement of the top cover.

In soil mechanics, annular shear cell was replaced by shear apparatus to study the stress–strain properties until failure. The shear apparatus was outperformed later in practice by more versatile triaxial machine coupled with the ability to measure global and local volumetric strain with various techniques. Nevertheless, very few experimental studies on glass beads were investigated. Stick–slips were observed with strong dilatancy effect in high confining pressure in experiments of the pioneer works of Kim [34]. Adjemian [1] presented the first systematic study of stick–slip phenomenon on dry glass beads in triaxial compression in the lower range (30–60 kPa) of confining pressure and evidenced some occurring conditions of slow vertical strain rate, lower density and specimens with small grain to sample diameter, small height to sample diameter. Roussel [60] extended the previous results on medium to dense dry glass beads over the range of 100–400 kPa and showed no evidence for single or multiple shear bands with CT images, contrasting the case of dense sands [13]. In a previous work [16], very large quasi-periodic stick–slips exhibited unpredictable shear stress breakdown to the initial isotropic level and coupled with simultaneous volumetric strain on fully saturated granular media. In drained condition, stick–slip behaviours on loose samples strongly resembled the hardening response of dense granular sample, including the dilatancy characteristic at large strain. Additionally, a unique stress–dilatancy relation applies to all stick–slip events.

Some main questions concerning the stick–slip instability persist: what are the triggering mechanisms and how large is the role of pore pressure, especially for fully saturated media? More importantly, is the presence of **shear stress** a mandatory condition? Despite recent experiments performed on simpler 2D granular media consisting of photo-elastic polymer discs [7] or 1D cylinders [58], these questions remain unsolved and the stick–slip phenomenon largely unnoticed by DEM experiments. The particular cases of isotropic loading, monotonic or cyclic, are unfairly ignored in experiments. Nevertheless, Lagioia and Nova [38] showed a rare known case of de-structuration on calcarenite in isotropic compression, with unknown dynamic features. It represents a transition from rock-like to soil-like behaviour with large void ratio drop at high isotropic stress.

Up to now, the stick–slip phenomenon in triaxial compression shearing still remains an elude subject for theoretical, numerical and experimental scientists. The discovery of isotropic liquefaction for the same model granular materials in our previous works had thickened the mystery [15, 19]. The main findings were the spontaneous liquefaction under undetermined external isotropic stress, associated with three necessary conditions and

liquefaction-free for dense state below a threshold void ratio at fabrication e_{30}^{liq} , representing the transition from global instability with total failure to local instability with partial collapse.

Since it opens the possibility of new mode liquefaction for natural granular materials probably in improbable places, it is worth to explore thoroughly the local collapses leading to this isotropic liquefaction. Tracing back how the instability evolves, especially the excess pore fluid pressure, may reveal insights into different inner components of isotropic liquefaction, previously unsuspected and even now still partially understood. Since the experimentalists often overlook the compressibility behaviour of loose, ideal granular materials in very simple condition of triaxial **isotropic drained** compression or isotropic consolidation, the purpose of this paper is to investigate the unknown and presumably uninteresting mechanical behaviour of these analogue materials, without any external shearing component; and letting aside the spectacular events of liquefaction. It presents new unconventional experimental findings of a comprehensive programme on very loose and saturated monodisperse glass beads beside a brief report on preliminary salient features [18]. It reports in-depth observations leading to a collapse-free behaviour below a threshold void ratio at fabrication e_{30}^{col} , the instabilities of normally consolidated and overconsolidated state under isotropic cycles and the associated dynamic characteristics. Only the effects of effective isotropic stress are considered in this paper. Mono-sized glass bead samples were prepared by moist-tamping technique and isotropically compressed with constant stress rate. Although glass beads are specific granular materials, they may activate some mechanisms usually hidden or partially developed in real granular soils.

Section 2 describes the experimental programme including the idealized material and the sets of the laboratory tests. The global compressibility behaviour under isotropic or one-dimensional compression is strongly affected by unexpected “stick–slip”-like events. These remarkable isotropic instabilities of a typical experiment are reported in Sect. 3. The analysis of these spontaneous dynamic events in compression loading, including some rare events in compression unloading, is presented in Sect. 4, together with their dependence on the initial void ratio and triggered isotropic stress and some possible driving physical mechanisms. Finally, the paper highlights the essential conclusions in the last section.

2 Experimental programme

The experimental works are conducted using a modified classical triaxial cell shown in Fig. 1. All samples are isotropically compressed in a manually stress-controlled mode with approximately constant total stress rate. The

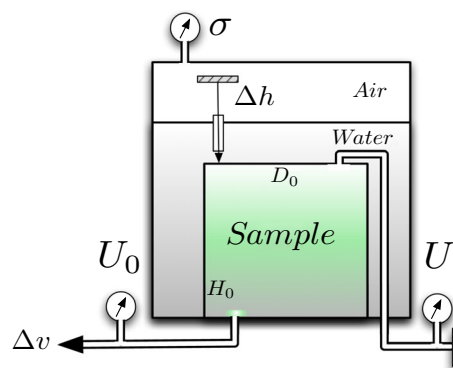


Fig. 1 Sketch of the experimental setup for isotropic compression

axial displacement Δh is measured by a linear variable differential transformer (LVDT) sensor mounted directly on the top platen. The global axial strain is estimated from $\varepsilon_a = \Delta h/H_0$ with H_0 the initial height. The global volumetric strain is deduced from $\varepsilon_v = \Delta v/V_0$, where V_0 is the initial sample volume and the water volume Δv expelled from or moved into the sample during isotropic compression. The water volume Δv is converted from the displacement of a membrane along a calibrated tube measured by another LVDT sensor. The pore water pressure U is recorded by a transducer outside the triaxial cell using very thick plastic tube connected to the top cap of the granular sample, at a distance of about 60 cm, since the constant back pressure U_0 needed for a full saturation is applied at the bottom of the sample. The sample preparation, the saturation procedure, the initial void ratio determination by two independent methods, the verification of the anti-frictional system are given in previous works on sands [17]. The current effective resolution including actual sensors, electrical cables, data acquisition systems of all transducers are carefully evaluated: ± 0.05 kPa for the pore and isotropic cell pressure, $\pm 1.4 \times 10^{-6}$ for axial strain and $\pm 0.8 \cdot 10^{-5}$ for volumetric strain.

Industrial soda-lime spherical glass beads “Sil-glass” used in this experimental study were commercialized by CVP, Linselles, France.¹ After the elimination of the small amount of beads smaller than 0.3 mm of diameter, a nearly unimodal population is obtained. Figure 2 presents the grain size distribution using particle size analyser performed by laser diffraction showing clean and poorly graded fine-grained granular media, the frequency histogram with a slightly asymmetric distribution and the image of virgin spherical glass beads SLG 6-8 viewed under SEM (scanning electron microscopy). These glass beads have a static friction coefficient of 0.24 on glass, according to CVP. The usual index properties are reported in Table 1.

¹ www.Cvp-abrasif-broyage.com.

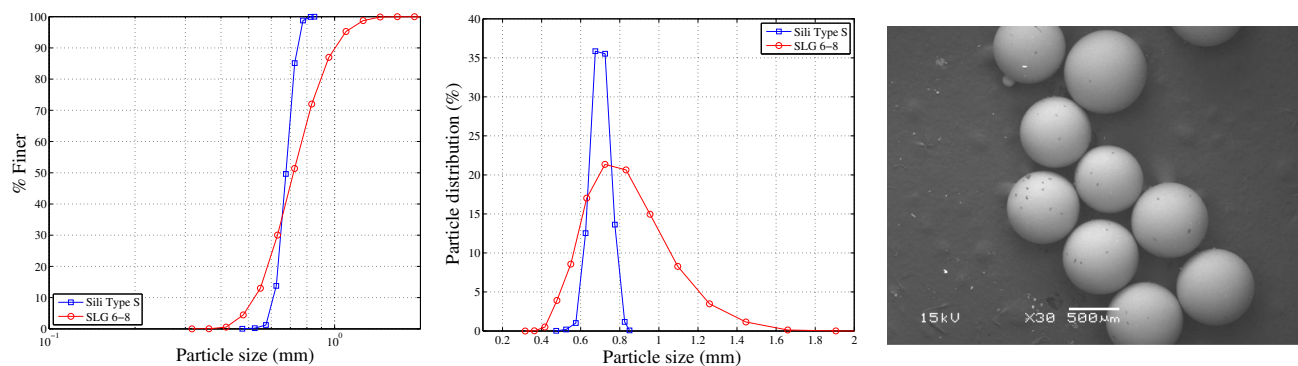


Fig. 2 Particle size distribution, frequency histogram and SEM image of SLG 6-8 glass beads of 0.7 mm of diameter

Table 1 Index properties of SLG 6-8 glass beads

Property	Value
Specific gravity, ρ_s	2.50
Mean size, D_{50} (mm)	0.723
Uniformity coefficient, C_u	1.463
Curvature coefficient, C_c	0.989
Maximum void ratio, e_{\max}	0.686
Minimum void ratio, e_{\min}	0.574

Short cylindrical sample, $H_0 = 70$ mm in height and $D_0 = 70$ mm in diameter, enclosed within a 0.3-mm latex membrane is prepared using a modified moist-tamping and under-compaction method [8, 36] to create loose and contractive granular samples. Enlarged end plates are used to produce homogeneous deformations at large strains during shear. Predetermined quantities of moist glass beads, mixed with 2% of distilled water in weight, are placed and gently compacted in five layers of prescribed thickness using a flat-bottom tamping circular stainless steel rod of 20 mm in diameter. Special care was given to have samples with nearly identical void ratios at fabrication state to minimize the well-known effect of density on the observed behaviour. To obtain a fully saturated state, CO_2 method [37] with de-aired distilled water, and back pressure of up to 200 kPa were applied. The resulting Skempton's coefficient $B = \Delta U / \Delta \sigma \geq 0.95$ indicates a fully saturated sample [63]. To avoid possible wearing effects, only virgin glass beads were used.

The void ratio of each granular sample was carefully evaluated from the water content obtained at the end of the isotropic compression or the shear loading [73], and also from the usual procedure of measuring the sample dimensions during different fabrication stages.

Two sets of drained isotropic compression tests were designed to study the unconventional instability phenomenon of idealized, fully saturated and very loose model granular materials: the first series of normally consolidated

and very loose samples to inspect the triggering condition of the unusual isotropic collapse up to 500 kPa, the second series of overconsolidated samples with $OCR = 4$ and $\sigma'_{\max} = 400$ kPa and decreasing void ratio to study the effects of initial void ratio and to identify the threshold void ratio at the beginning of isotropic consolidation at 30 kPa e_{30}^{col} , leading to a collapse-free behaviour during isotropic compression. A complementary test is performed to compare the newly discovered isotropic instability with the stick-slip instability in drained compression. Some additional tests with a few isotropic cycles are also conducted to study the preliminary effects of isotropic cycles. The average initial void ratio at fabrication state, e_0 , of the first series was around 0.713 (solid fraction $\Phi = 0.584$) or a relative density D_r of -24% giving an artificially very loose sample. The initial bulk density is of about 1.428 g/cm^3 .

Table 2 summarizes the selected tests of this study with their initial conditions and their results. e_{30} (respt. Dr_{30}) is the void ratio (respt. relative density) at the beginning of isotropic consolidation at 30 kPa. σ'_{trig} represents the value of applied effective isotropic pressure for the accident having the largest void ratio reduction Δe . $\Delta \varepsilon_v$ is the incremental volumetric strain, $\Delta \varepsilon_a$ the incremental axial strain produced during the event, ΔU_{peak} the peak of excess pore pressure in transient phase, ΔU_{stable} its stabilized value after this transient phase, f the frequency of the transient phase of pore pressure buildup, C_c the compression index, C_s the swelling index, $i_{\text{stat}} = \frac{\Delta \varepsilon_v}{\Delta \varepsilon_a}$ the incremental anisotropic coefficient in quasi-static consolidation, C_p the wetting induced collapse potential and t_{50} the time for 50% of consolidation.

3 Typical experimental results

Due to the undetermined nature of the triggering stress and the unpredictable character of the observed instabilities [19], it is worth to examine in some details the local collapses without global liquefaction of a typical test.

Table 2 Isotropic consolidation tests on very loose and idealized granular materials

Tests	$e_{30}(Dr_{30})$ (kPa)	σ'_{trig} (%)	Δe (10^{-2})	$\Delta \varepsilon_v$ (%)	$\Delta \varepsilon_a$ (%)	ΔU_{peak} (kPa)	ΔU_{stable} (kPa)	f (Hz)	C_c (10^{-2})	C_s (10^{-2})	i_{stat}	C_p (%)	t_{50} (s)
Series A : Isotropically Normally Consolidated, OCR = 1, largest void ratio drop Δe													
N1	0.671 (13.4)	395	1.48	0.82	-0.275	428	348	105	1.84	1.21	20.0	0.472	0.678
N2	0.699 (-11.6)	275	1.92	1.13	0.053	476	256	106	1.73	1.21	20.1	-0.044	1.392
N3	0.724 (-33.9)	146	0.98	0.59	0.207	222	111	111	1.75	1.47	15.5	0.266	1.283
N4	0.688 (-1.8)	117	0.61	0.42	0.023	145	73	78	1.67	1.35	19.0	0.000	1.149
N5	0.783 (-86.6)	188	1.12	0.566	-0.073	315	146	92	1.69	1.43	18.5	-0.073	0.502
Series B : Isotropically Overconsolidated, OCR = 4													
S1	0.690 (-3.6)	274	1.60	0.89	0.114	408	240	46	1.93	1.37	14.3	0.219	1.121
S2	0.677 (8.4)	310	1.30	0.74	-0.201	**	**	**	1.59	1.59	12.4	0.752	0.767
S3	0.632 (8.4)	152	1.10	0.63	0.131	271	133	105	1.53	1.53	9.5	0.231	0.865
S4	0.608 (8.4)	122	0.70	0.41	0.033	69	69	104	1.53	1.53	17.4	-0.002	0.890
Isotropic Cycles													
S5	0.654 (28.6)	169	2.03	1.231	0.119	174	87	90	1.79	1.63	19.1	-0.040	0.622
S6	0.707 (-18.8)	93	0.80	0.357	0.165	144	65	39	1.79	1.75	18.3	-0.022	1.632
Dense Dry Deposition													
SP1	0.596 (80.3)	89	0.10	0.045	0.021	17	8	98	1.78	1.44	15.7	0.000	0.218
SP2	0.584 (91.1)	-	-	-	-	-	-	-	1.63	1.41	-	-0.047	-
Moist Sample													
SP3	0.700 (-12.9)	45	-	-	0.335	2.1	0.6	-	-	-	-	-	0.218

** No oscillating pore pressure in transient phase

For isotropic consolidation testing, the results were examined mainly in the traditional semi-logarithmic compression plane $e - \log \sigma'$. To clarify the unusual behaviour, the time evolution of σ' , ε_v , ε_a and ΔU were added. Following the usual convention in soil mechanics, volumetric (respt. axial) strains are positive for compaction (respt. contraction).

3.1 Unusual spontaneous accidents, stick–slip in isotropic consolidation

Figure 3 shows a typical triaxial isotropic compressibility behaviour from 30 to 400 kPa of idealized and loose granular materials for a typical example of test N1 having $e_{30} = 0.671$. Small red arrows indicate the time direction. The behaviour measured by the usual slow and non-synchronized acquisition system at 0.5 Hz (red dashed line and hollow circles) is superimposed with that of fast filtered and synchronized one at 2048 Hz (blue line).

Instead of an expected continuous and linearly decrease of e with increasing σ' in the compression diagram, several accidents, labelled as events A to D with large accidental drops Δe (event B will be addressed later), interrupt the usually smooth macroscopic compressibility behaviour. Each accident consists of a sudden and rapid reduction of σ' at the beginning of each event, followed by an equally rapid recovery to the previous effective stress level in less

than 4 s as in the case of event A and the linear isotropic consolidation resumes afterwards until the next accident. The measured isotropic triggering stress σ'_{trig} is successively at 67, 68, 152 and 395 kPa.

These irregular events, or unusual accidents, can be characterized by three macroscopic parameters: a simultaneous and fast volumetric compaction $\Delta \varepsilon_v$ and axial contraction $\Delta \varepsilon_a$, excepting for event E, and an equally simultaneous and spontaneous increase of ΔU or decrease of σ' , followed by a gradual dissipation of ΔU or slowly recovery of σ' , according to the effective stress principle. These events are termed as local collapses, strongly resembling the stick–slip phenomenon in triaxial shearing. Since they leave intact the cylindrical form of the specimen, at least visually, the subsequent usual triaxial sheared test in compression or in extension can be performed, either in drained or in undrained condition [2, 5, 16]. Distinct audible cracking noises were systematically heard before the appearance of sudden small variation of ε_v or sometimes the spontaneous generation of ΔU on the controlled screen.

3.2 Unexpected excess pore pressure

At the beginning of each event, σ' was first reduced to a small value below 1 kPa and seemed to oscillate at constant void ratio by the presence of multiple fast folding

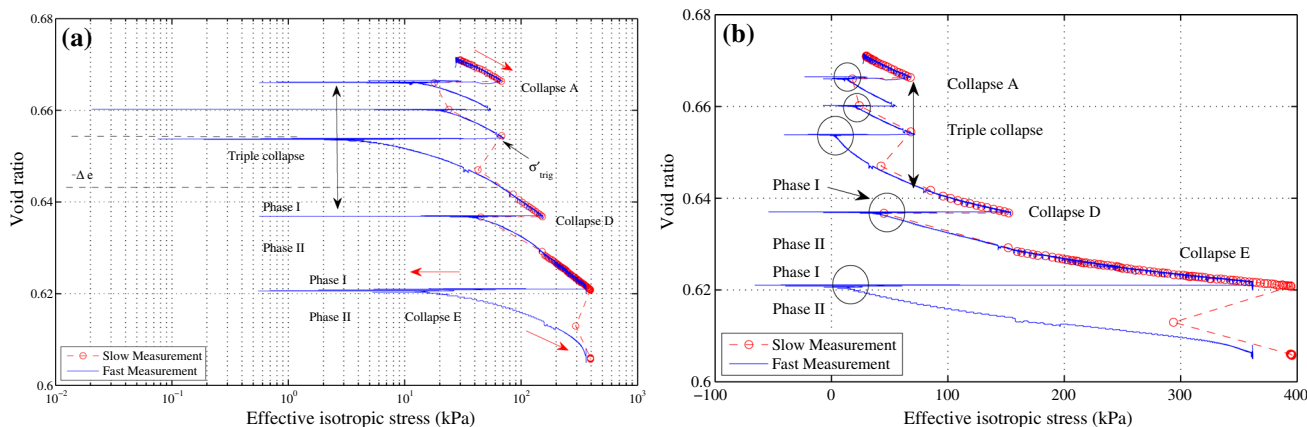


Fig. 3 Spontaneous collapses under isotropic consolidation of test N1, $e_{30} = 0.671$, with slow and fast measurements: **a** semi-logarithmic plot, **b** linear plot (colour figure online)

horizontal lines in Fig. 3a; then began to recover gradually with a gently curved behaviour, completing the missing data acquired with the slow acquisition system. Short-lived event B has little chance to be detected by slow system, and since the σ'_{trig} of event B remains within the dissipation range of event A, events A and B can be qualified as a double collapse and even events A, B and C a triple collapse.

Since the semi-logarithmic plot cannot represent the eventually unexpected large positive spikes of measured pore water pressure, or large negative spikes of σ' , the alternate linear scale in Fig. 3b for σ' reveals the full extend of ΔU or σ' . The σ' is briefly negative for all events, even down to -75 kPa for the last event E.

Typical evolution of ΔU (large black hollow circles) of each event can be decomposed in two phases: a first and fast transient oscillatory phase *I*, suddenly developed from a previous steady state, at practically constant volume with large spikes ΔU_{peak} , until attaining the briefly stabilized ΔU_{stable} and a second and longest phase *II* of excess pore water pressure dissipation at nearly constant ϵ_a and ϵ_v towards the initial steady-state back pressure. Despite the fully drained system, phase *I* occurs practically in undrained conditions and phase *II* in drained conditions.

3.3 Dynamical events

Figure 4 provides the complete time evolution of ϵ_v , ϵ_a , ΔU and cell pressure σ of accident A during transient oscillatory phase *I*. The time origin is shifted to the beginning of the sudden development of ΔU with an error of ± 0.5 ms of the current time resolution.

A time delay of about 20 ms is noticed between the sudden rise of ΔU and the beginning of the gradual progression of ϵ_a . In this figure, ΔU can be seen as the initial cause of the development of ϵ_v and ϵ_a in the following

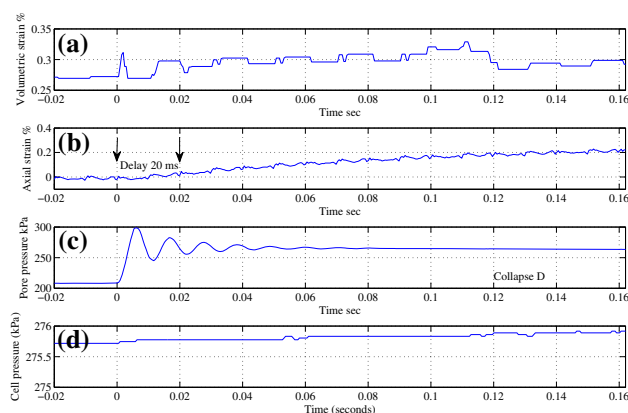


Fig. 4 Time evolution of volumetric strain (a), axial strain (b), pore water pressure (c) and cell pressure (d) of event A occurring at 67 kPa of test N1

sequence for a local liquefaction: an increase in ΔU means a decrease in σ' for a fully saturated media, consequently a reduction in strength and a global growing progression of ϵ_v and ϵ_a to a stabilized value due to the recovering of σ' to the previous level. However, this sequence points out to a logical question: how and when ΔU be triggered? In other words, what are the triggering mechanisms for these unexpected collapses?

A stiff dynamic pore pressure sensor with high resonant frequency (250 kHz) was used together with the static one to check the reliability of the transient phase *I*. The brief vibration of ΔU is clearly not an artefact of the measurement system since no difference was detected between two systems. Additional verifications are also done to check the effects of environmental disturbances on the measuring system.

In this experiment, all collapses terminate the oscillating phase *I* with a briefly stable value ΔU_{stable} (nearly without oscillations) before commencing the dissipating phase *II*

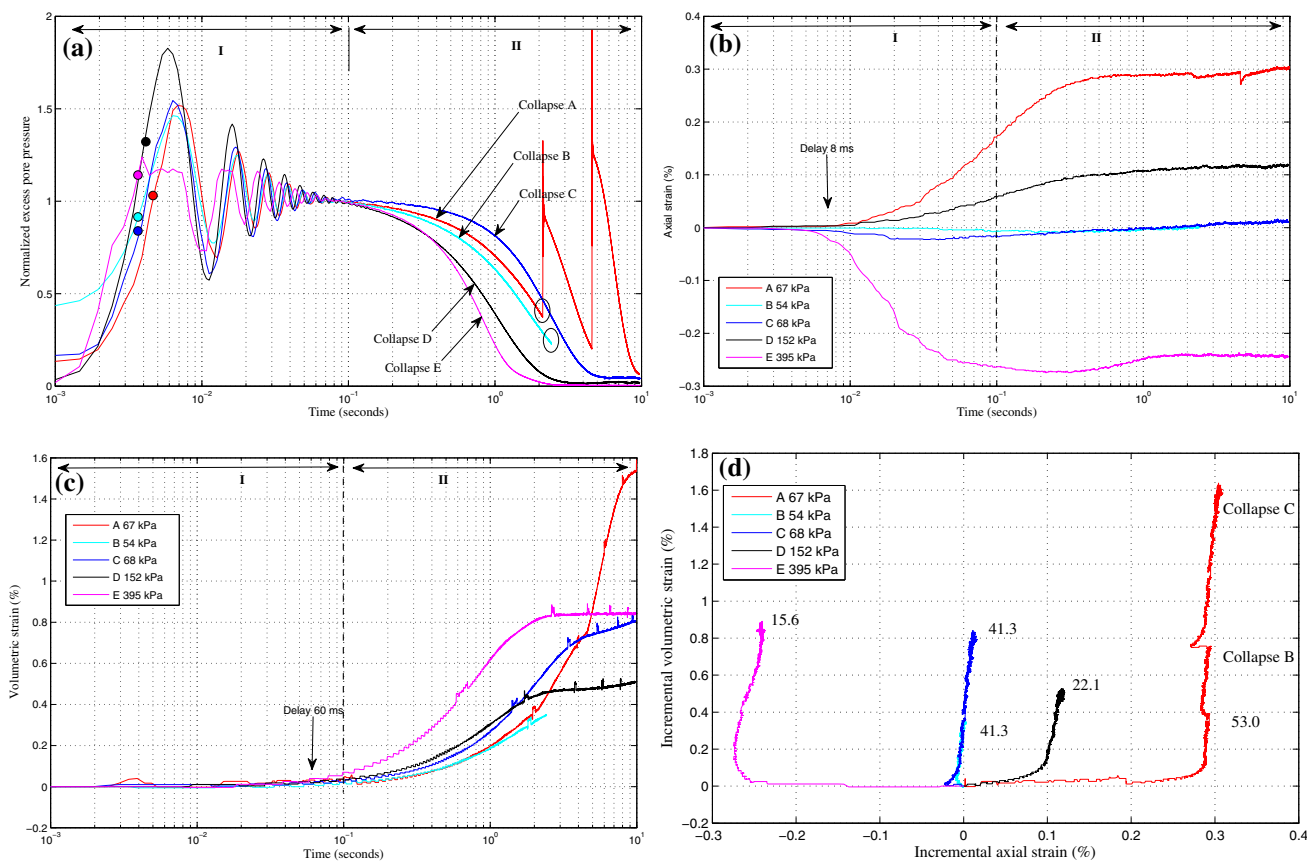


Fig. 5 Time evolution of isotropic collapses and after-collapses of test N1. **a** Two phases of normalized excess pore pressure: I fast buildup and II dissipation for all events with inferred liquefaction state (*solid circles*), **b** axial strain, **c** volumetric strain, **d** Relationship between incremental volumetric and axial strain, *black numbers* indicate the dynamic incremental anisotropic coefficient i_{dyn} in the transient phase (colour figure online)

due to the drainage system. The normalization by the stabilizing value of ΔU_{stable} is a convenient procedure to eliminate the eventual dependence on ΔU_{stable} .

Figure 5a groups together ΔU^{norm} for all normalized events in a semi-logarithmic time scale to emphasize the transient phase I and gives a complete evolution of ΔU . This time evolution indicates a clear separation of the two regimes at about 100 ms: fast transient below and slow dissipation above. The two small black hollow circles at 2 s illustrate the abrupt termination of events A and B and the sudden generation of events B and C in a triple sequential event ABC. Despite different triggering times of events B and C in the middle of consolidation phase t_{50} of event A, all rise times happen rapidly in less than 4 ms in phase I and the consolidation created apparently from a loading step completes in less than 6 s in phase II. Different superimposed liquefaction points (*solid circles*) indicate the ΔU^{norm} levels corresponding to a null effective stress state close to unity, hence the short-lived local liquefaction with limited deformation, contrasting the normal full global liquefaction with runaway deformation [15, 19].

Without double event B and C, called after-collapses, the pore pressure dissipation of event A can be terminated normally at about 5 s; with ϵ_a remains practically constant during subsequent events B and C, while ϵ_v continues to evolve steadily with an accelerated pace with event C. Successive collapses can be interpreted as aftershocks in earthquake engineering. This triple collapse strengthens the previous asked question for triggering mechanisms.

All single collapses and the first events of a set of multi-collapses (double, triple collapses, ...) occur under constant isotropic stress rate of about 0.07 kPa/s. Events B, C happen in the process of dissipation of pore pressure which is equivalent to an increase in effective stress; meaning a faster increasing stress rate of 44.74 kPa/s. This suggests a stress rate-independent feature for the mechanical behaviour during collapses.

The isotropic consolidation regime of phase II gives strongly an impression of déjà vu. Similar to the traditional one-dimensional consolidation in soil mechanics, two additional macro-parameters can be identified [66]: the time t_{50} for 50% consolidation and the slope C of the

Table 3 Dynamic characteristics under drained isotropic compression of test N1, $e_{30} = 0.671$ ($Dr = 13.4\%$). Osc is the number of oscillations, Stab the stabilization time and Dis the dissipation time

Event	σ'_{trig} (kPa)	ΔU_{max} (kPa)	ΔU_{stable} (kPa)	Osc.	f (Hz)	Sta. (ms)	Dis. (s)	Offset (ms)	e_{trig}	Slope C	t_{50} (s)	Δe	$\Delta \varepsilon_v$ (%)	$\Delta \varepsilon_a$ (%)
A	67	99	65	8	93.1	100	–	0	0.666	1.183	1.667	0.0076	1.421	0.289
B	54	86	59	8	93.1	100	–	0	0.660	1.054	1.368	–	–	–
C	68	125	81	8	102.4	100	6	0	0.654	1.495	2.006	–	–	–
D	152	210	115	10	97.5	100	4	20	0.637	1.183	0.808	0.0148	0.465	0.115
E	395	≥ 428	346	8	93.1	100	3	18	0.621	1.742	0.676	0.0148	0.818	–0.275

straight portion of the consolidation curve. Table 3 gives the dynamic characteristics for all events of test N1.

The ε_a and ε_v for all collapses are shown in Fig. 5b, c, with the origin shifted to the steady-state value before collapse event to avoid clumsy figures. The lack of simultaneity between ΔU or σ' and ε_a , ε_v is one of the characteristics of these sudden collapses.

Figure 5b reveals a fast and progressive axial contraction towards a stable value of 0.28% within only 0.6 s. It indicates a dynamic regime of the local collapse. The volumetric contraction occurs at constant axial strain in the dissipated regime of phase II, indicating a particular anisotropic deformation under isotropic stress. While subsequent collapses B and C induce very little axial strain, continuous volumetric contraction suggests a strong successive structural rearrangements with emphasis on the horizontal direction.

For dynamic collapses, the incremental relationship between $\Delta \varepsilon_v$ and $\Delta \varepsilon_a$ in Fig. 5d below 10 s evolves rapidly towards straight line, even for the surprising axial extension case of event E. These relations give large dynamic incremental anisotropic coefficient $i_{\text{dyn}} = \Delta \varepsilon_v / \Delta \varepsilon_a$ during the transient phase, depending on each collapse, because $\Delta \varepsilon_v$ occurs essentially at constant axial strain, nearly after completion of $\Delta \varepsilon_a$, even for after-collapses. Small effective stresses of collapses A to C tend to have large value of i_{dyn} . The initial flat segment around null $\Delta \varepsilon_v$ denotes the initial time delay compared to $\Delta \varepsilon_a$. The value $i_{\text{dyn}} = 22.1$ of collapse D approaches the static one of Sect. 3.4.

3.4 Compressibility parameters

This drained isotropic compression test presents a dramatic departure from classical results. While the overall effects still have globally a volumetric compaction, it features a new set of randomized accidents, altering apparently the compressibility behaviour. However, in Fig. 6, if the four loading phases preceding the collapse event are retrieved and artificially shifting upwards at σ'_{trig} by Δe from Fig. 3, a new compressibility curve, surprisingly continuous, is created without phases I and II. This construction closes the

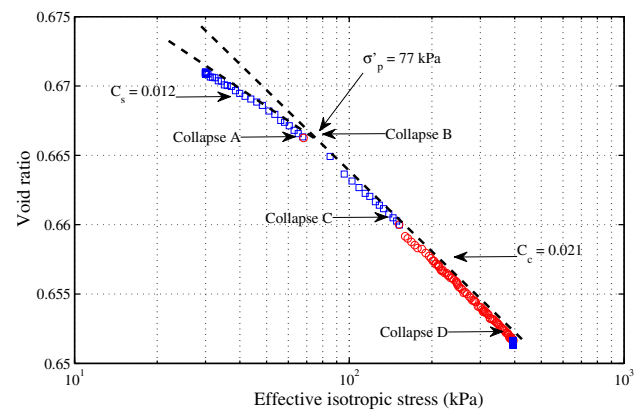


Fig. 6 Classical compressibility parameters under isotropic consolidation from 30 to 400 kPa of test N1, upon ignoring dynamic collapses by artificially shifting upwards at σ'_{trig} by Δe

void ratio gap created by spontaneous collapses and linking together four largest linear segments and reveals a hypothetical mechanical behaviour conforming to the usual isotropic or 1D compressibility of loose sand materials without unloading under fully drained conditions [75]. In soil mechanics, the compressibility behaviour of virgin materials can be approximated by two superimposed straight dashed lines in Fig. 6 representing the normal virgin compression line (VCL) and the unloading-reloading line. The initial slope of the curve has approximately the same value as the unloading line. The intersection point of these two lines defines an apparent preconsolidation stress σ'_p as a reminder of the past maximum effective stress. The true σ'_p can have higher value due to the under-compaction technique.

Using this construction, some macroscopic compressibility parameters can be identified: a compression index $C_c = \Delta e / \Delta \log \sigma' = 0.021$ for loading, a swelling index $C_s = 0.012$ for approximating the unloading and an apparent preconsolidation stress $\sigma'_p = 77$ kPa created logically by the under-compaction method. This specimen of loose glass beads has a particular drained isotropic compression behaviour with $C_s \approx C_c/2$, in contrast with real granular

materials where $C_s \approx C_c/10$. This observation suggests a quasi-reversibility behaviour for model granular materials numerically obtained in [3, 35, 62] with monodispersed spherical particles, upon ignoring the unexpected dynamic collapses.

Without these collapses, the void ratio at the end of isotropic consolidation at 400 kPa would be in a medium state of $e_c = 0.652$ ($Dr_c = 30.4\%$), instead of a dense state of $e_c = 0.606$ ($Dr_c = 71.4\%$). It means the impossibility to control the void ratio reduction in isotropic consolidation due to random occurrence of spontaneous collapses, unless mastering the triggering mechanisms.

The same moist-tamping procedure gives a rather large $i_{stat} = 20$ on monodispersed loose glass beads during isotropic consolidation, contrasting sharply the isotropic structure with $i_{stat} \approx 3.0$ for loose laboratory sands (i.e. Hostun or Toyoura) [24]. This surprisingly strong initial structural anisotropy of an assembly of spherical particles could result from preferred orientation of unit vectors normal to contact surfaces [50], or the results of local shear stress generated by isotropic compression from DEM numerical simulations, although with crushing mechanisms on a dense media [45]. It is currently hypothesized as one of the leading key component in the creation of observed instabilities.

4 Analysis of spontaneous dynamic collapse

After the description of experimental evidences of a typical investigation, we will now focus on the global analysis of these unconventional dynamic instabilities of fully saturated, normally consolidated and overconsolidated glass bead material subjected to isotropic drained compression and on the **speculation** about the possible driving physical mechanisms behind.

4.1 Random instantaneous collapses and instabilities

A set of 4 additional tests of series A having very loose density was performed to study the occurrence of isotropic triggering stress σ'_{trig} in Fig. 7, with double collapse and isotropic cyclic loadings of test N5.

Some experimental observations can be made from this series. The most obvious is the persistent presence of numerous collapses with local liquefaction for all tests; the second observation concerns the undetermined nature of σ'_{trig} with an uneven distribution in the studied range from 30 to 400 kPa; the third confirms the quasi-elastic behaviour with $C_s \approx C_c$, associated with small hysteresis loop in Fig. 7a and the last one points to the absence of

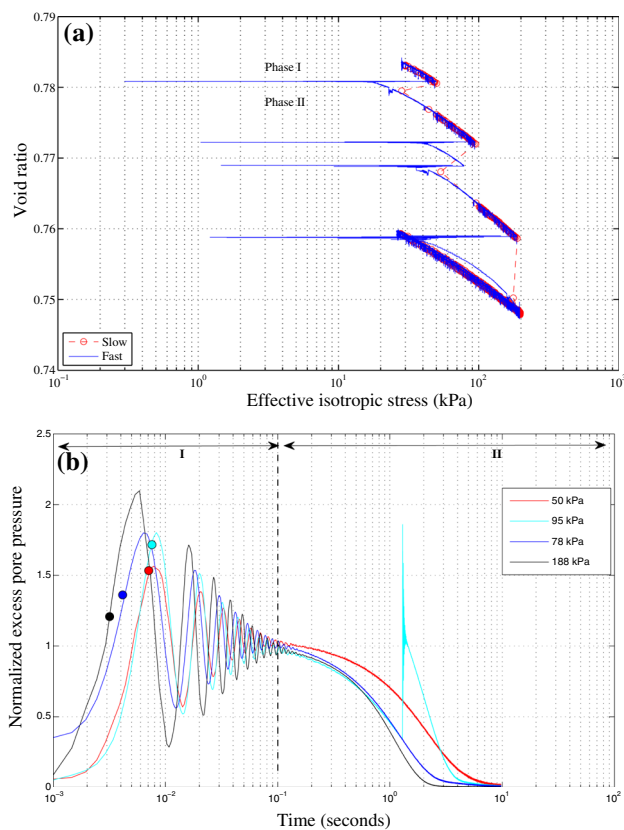


Fig. 7 Isotropic consolidation from 30 to 400 kPa and pore pressure evolution of dynamic collapses of test N5 ($e_{30} = 0.783$)

collapse during at least two isotropic cycles. If the granular assembly can support up to a given effective stress; then, the resulting microstructure can support any stress below this maximal attained level; therefore, the last observation is logically expected for overconsolidated sample. These observations seem to suggest a new characteristic of loose model granular assemblies in isotropic consolidation.

For clarity, Fig 7b shows separately the time evolution of ΔU^{norm} . The inferred liquefaction levels (solid circles), all well above the unit normalized level, point to a very short-lived liquefaction state, hence to the existence of local collapse. Note the rare double successive collapses for the loosest sample, the smallest t_{50} and the fastest dissipation time in this series. As in the case of triple collapse of test N1, the second collapse also happens within the dissipation range of previous event.

Visually, no sign of strain localization was noticed in these experiments, partly due to small strains created by isotropic compression below 400 kPa. Nevertheless, advanced X-ray tomography can detect the invisible multiple localized deformation deep inside the sample [13, 31]. The observed dynamic instabilities might be related to the

diffuse failure for undrained [12] and drained [59] shear behaviour for loose granular material.

With the use of pore fluids having higher viscosity [9], other than pure water, the possibility and the occurrence of collapse could be different. However, this particular aspect is left for future studies.

4.2 Effects of changes in σ'_{trig}

Figure 8 displays the dependency of σ'_{trig} on the measured macroscopic parameters of each event, $\Delta\varepsilon_v$, $\Delta\varepsilon_a$, ΔU_{peak}

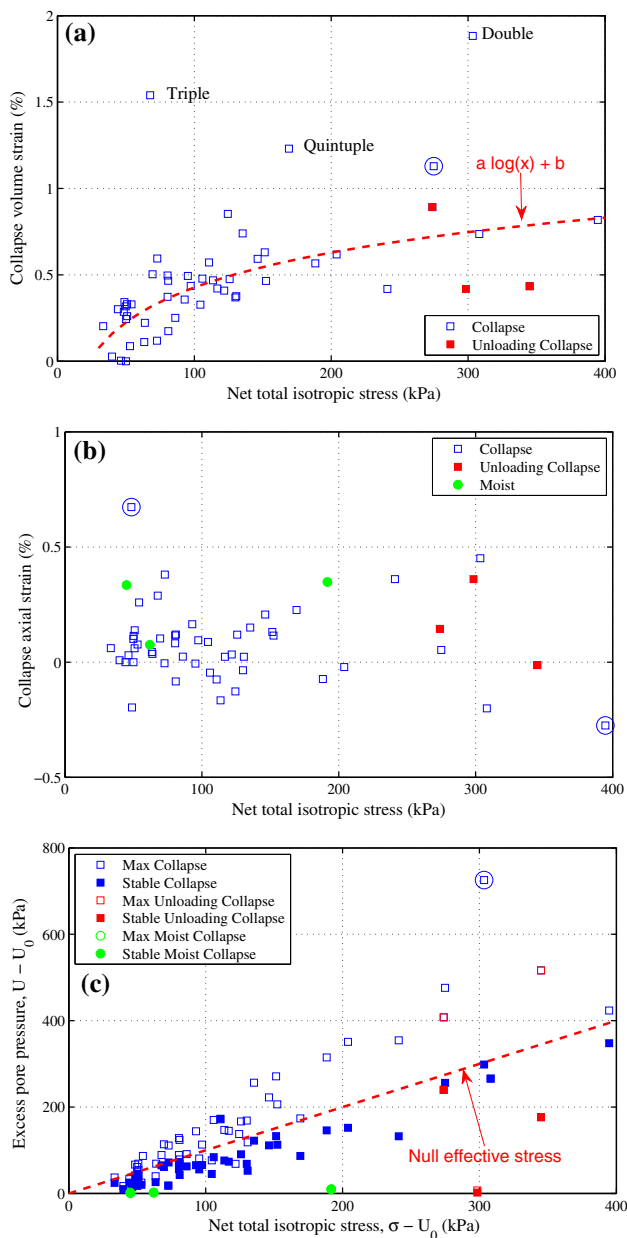


Fig. 8 Effects of σ'_{trig} on isotropic collapses. **a** Collapse volumetric strain, **b** collapse axial strain, **c** excess pore pressure (colour figure online)

and ΔU_{stable} for the whole set of 64 collapses collected from 25 isotropic compression tests. The additional unloading and moist collapses will be examined later in Sect. 4.4. Figure 8a suggests an approximately logarithmic increasing trend of $\Delta\varepsilon_v$, with reasonable correlation factor of 0.743, without multiple collapses (double, triple and quintuple). Large confining effective pressure tends to create fewer accidents with large volumetric compaction limited by a value below 1%. About one-third of all collapses presents surprisingly small axial extension in Fig. 8b, scattering all over the whole range of σ' , instead of the usual compression state for an increasing isotropic stress loading. This particular axial extension can be probably related to the inclination of the top plate, therefore, to the inhomogeneous state of specimen. It indicates a high anisotropic strain state. It seems that σ'_{trig} was randomly distributed over the range of studied effective confining stress, from 30 to 400 kPa, with a dominant group below 200 kPa. It can be as small as 33 kPa without any preceding local collapses, or as large as 394 kPa with numerous preceding local collapses or precursors.

Two characteristics of ΔU in the transient phase, ΔU_{peak} (hollow symbols) and ΔU_{stable} (solid symbols), are plotted together in Fig. 8c. While the short-lived ΔU_{peak} is often located above the diagonal red line representing the liquefaction state of null effective stress where the excess pore pressure ΔU equals the net total confining pressure $\sigma - U_0$, most of the stable value ΔU_{stable} remain below or near this line. The current leading hypothesis is that the brief duration of the transient phase *I* in the range of 100 ms is enough to initiate local liquefaction, but not enough to maintain its development and to propagate the liquefaction state to the whole sample. The stabilized value ΔU_{stable} , located below the liquefaction line, gives a small and however positive σ' , which is enough to stop immediately this local liquefaction state. A separation of beads can occur during this short-lived and small σ' , but it lasts during a too short period to activate the role of gravity in the dynamic phase *I*. If this period is prolonged for more than one second, the current granular skeleton is destroyed and liquefaction will follow.

Only three rare unloading collapses at high stress (red) and three moist collapses (green symbols) from two additional tests are conveniently inserted within the trend of these figures with comparable collapse axial and volumetric strains. Small pore air pressure is detected for moist and unsaturated samples. It suggests two important facts despite the small number of additional experiments: the fragility and metastability of the obtained microstructure on very loose idealized granular assemblies, and the unnecessary presence of the full pore water fluid to trigger these collapses.

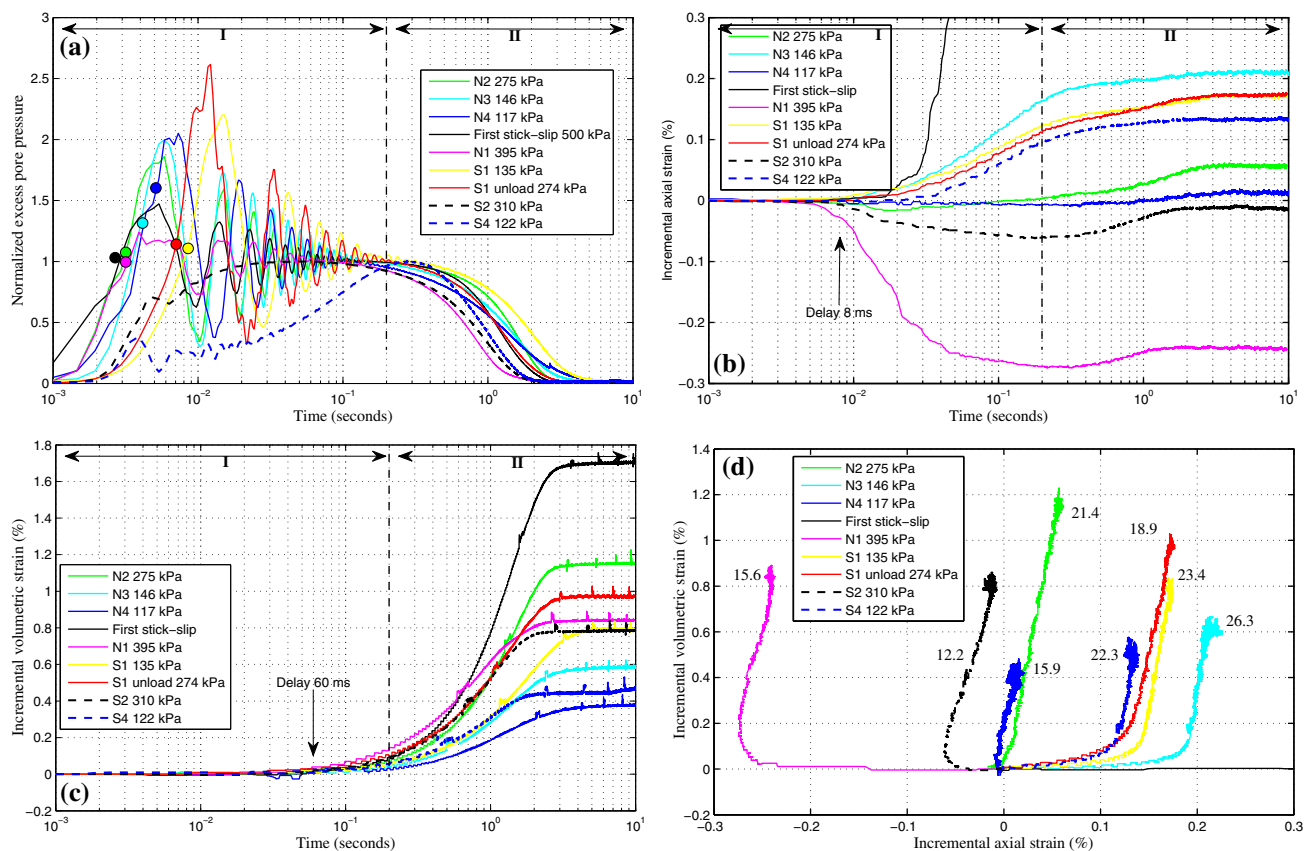


Fig. 9 Time evolution of largest isotropic collapses in compression, compared with rare unloading collapse and first drained compression shear stick–slip under 500 kPa. **a** Two phases of pore pressure development with inferred liquefaction state (*solid circles*), **b** incremental axial strain, **c** incremental volumetric strain, **d** relationship between incremental volumetric and axial strain. *Black numbers* indicate the dynamic incremental anisotropic coefficient i_{dyn} . The legend gives the triggering stress σ'_{trig} (colour figure online)

The largest jump (large circle with embedded square) of ε_v in a single collapse occurs at 275 kPa of test N2, the largest compression (extension) jump of ε_a at 48 (395) kPa of test S2 (N1), the largest and exceptionally large ΔU_{peak} happens at 303 kPa (test not shown) and ΔU_{peak}^{norm} for the unloading collapse at 345 kPa of test S6. Multiple collapses in cascade result in even large $\Delta \varepsilon_v$ at 169 kPa of test S5 (quintuple), at 68 kPa of test N1 (triple) and at 303 kPa (double), while leaving $\Delta \varepsilon_a$ inside the current trend. The scattering of these results reinforces the undetermined nature of σ'_{trig} , the unpredictability of axial and volumetric drops, the importance of cascading and unloading collapse and the lack of clear correlation between $\Delta \varepsilon_v$, $\Delta \varepsilon_a$ and ΔU_{peak} .

It is worth noting the wetting induced collapse potential $C_p = \Delta h/H_{wet}$ where Δh is the height variation during inundation with de-aired distilled water and H_{wet} the height at the beginning of saturation stage. It is the axial strain occurring during submersion and saturation by water. C_p is often used to quantify the collapsibility of metastable soils due to wetting in oedometric testing [71]. The collapse

potential for all tests in Table 2 is less than 1% which is the recognized limit for collapsible soils in oedometer. Consequently, very loose model granular assemblies are not prone to collapse on wetting and C_p is unable to detect the observed instability.

Upon ignoring all local collapses by artificially shifting upwards at σ'_{trig} by Δe , as in Sect. 3.4, a unique and global isotropic compressibility behaviour for model granular materials created by moist-tamping technique, independently of e_{30} , can be retrieved. Some mean values of the usual macroscopic compressibility parameters can be identified: $\langle C_c \rangle = 0.018$, $\langle C_s \rangle = 0.012$, $\langle \sigma'_p \rangle = 60$ kPa. The quasi-reversibility of compression behaviour is suggested by $\langle C_s \rangle \approx \langle C_c \rangle$.

4.3 Spontaneous collapse characteristics

Figure 9a shows the time evolution of ΔU^{norm} for the largest collapse of each test in Table 2, in terms of Δe , including the rare unloading collapse at 274 kPa of test S1 and the first stick–slip in drained compression at 500 kPa.

In the transient phase *I* for the first 100 to 200 ms, ΔU for loose assemblies (full line) mostly vibrates like an oscillating underdamped system with a dominant frequency mainly in the range of 100–110 Hz and disappears for denser ones (dashed line), although some high frequencies persist. These dashed lines emphasize the varieties and complexities of pore pressure development. However, the rising time to the first peak ΔU_{\max} is within 5 ms, followed by a relatively fast decay to stabilizing ΔU_{stable} . No suitable correlation can be established between $\Delta U_{\max}^{\text{norm}}$ and σ'_{trig} . The inferred liquefaction levels suggest a local liquefaction state for all vibrated transient phases and the absence of local liquefaction for non-vibrating ones. The subsequent longer dissipation phase *II* lasts within 4 s in which ΔU returns to the initial equilibrium $U = U_0$ at nearly constant axial strain. Despite the varieties of ΔU^{norm} in phase *I* and the range of σ'_{trig} from 117 to 395 kPa, all ΔU^{norm} are closely grouped together in a single dissipation curve within some experimental scatters.

ΔU^{norm} for the first drained shear stick–slip at 500 kPa of confining pressure (black thin line) has the same striking features of isotropic collapses, although with smaller peak; and that of unloading collapse (red thin line) has the largest $\Delta U_{\text{peak}}^{\text{norm}}$ and the lowest frequency. These nearly identical characteristics suggest probably a same underlying phenomenon, triggered by the same physical mechanisms independently of e_{30} and σ'_{trig} . It also seems that the striking pore pressure development is not the exception, it is the rule for local collapse in fully saturated granular media.

The corresponding $\Delta \varepsilon_a$ and $\Delta \varepsilon_v$ are shown in Fig. 9b, c. These figures emphasize the lack of simultaneity between ΔU or σ' and $\Delta \varepsilon_a$, $\Delta \varepsilon_v$ and the absence of oscillations in the transient phase for both $\Delta \varepsilon_a$ and $\Delta \varepsilon_v$. Instead of sudden axial and volumetric jumps often reported in the literature for stick–slip experiments [2, 5, 16, 32, 48], all tests in this time-resolved study offer a progressive and fast evolution of $\Delta \varepsilon_a$ and $\Delta \varepsilon_v$ from one steady-state value to another; even for the unusual case of negative $\Delta \varepsilon_a$. Incidentally, the first slip of the triaxial compression stick–slip offers the largest steady-state value for both $\Delta \varepsilon_a$ and $\Delta \varepsilon_v$.

For the selected accidents, the axial strain rate $\dot{\varepsilon}_a$ varies from 0.08%/s to a rapid rate of 1.16%/s while the volumetric strain rate $\dot{\varepsilon}_v$ changes from 0.36 to 2.37%/s. These rates suggest a dynamic regime of the collapse phenomenon in less than one (three) second for ε_a (ε_v). More than half of the $\Delta \varepsilon_a$ already happens during the transient phase *I* below 200 ms, essentially under undrained conditions of $\varepsilon_v \approx 0$.

The existence of ΔU^{norm} systematically detected as in Fig. 9a means in that short time period of the collapse event the pore pressure acquired at the top cap exceeds the

permanent back pressure U_0 imposed at the bottom creating the excess pore pressure which surges, oscillates and then returns to the steady U_0 . This implies a briefly non-homogeneous stress state inside the sample during the short-lived collapse for less than 4 s.

Figure 9d gives nearly parallel lines with a noticeable constant $i_{\text{dyn}} = 19.0 \pm 4.7$ in the dissipation phase *II* for all selected accidents, regardless of σ'_{trig} and of loading conditions (isotropic or shear, loading or unloading). The first stick–slip in Sect. 4.6 has a smaller value of 14.7 at $\Delta \varepsilon_a = 1.8\%$, not shown in this figure to emphasize the isotropic collapses.

Since the total time of liquefaction state ($\sigma' \approx 0$ kPa) is less than 0.5 s in Fig. 9a and the collapse axial strain less than 0.5% in Fig. 9b together with limited collapse volumetric strain, these collapses are termed as local liquefaction or local collapse with the original cylindrical shape maintained. A key question is “How long is the needed time to create a sustained high pore pressure for a global liquefaction state characterized by very large deformation?” and more importantly “What are the appropriate conditions to maintain these high pore pressure levels for a longer period?”. At this stage, no attempt has been conducted due to the still unknown triggering mechanisms of these events.

Figure 10a gives the effects of net total isotropic stress $\sigma - U_0$ on the duration of stabilized excess pore pressure for isotropic collapses. Excepting some rare cases, the stabilized ΔU lasts less than one second, irrespective to collapse state (loading, unloading, first or subsequent collapse). The dynamic incremental anisotropic coefficient i_{dyn} (blue) measured in the surge of U mostly coincides with the static one i_{stat} (red) in Fig. 10b. This observation suggests a same kinematic strain development for both quasi-static and dynamic phases.

4.4 Unloading collapse

One logical question arises instantly: Can these spontaneous macroscopic collapses happen in isotropic unloading? Following the current understanding of soil behaviour, the virgin isotropic consolidation line (VCL) suggests the existence of a stable domain in the compressibility diagram within which the soil behaviour can be considered as quasi-elastic and reversible with small hysteresis cycle [75]. This stable domain is located below VCL and the quasi-elastic behaviour reveals by overconsolidated test with an unloading–reloading cycle below a past maximum effective isotropic stress σ'_{max} . In other words, can the microstructure attained at σ'_{max} remain stable in an overconsolidated state below σ'_{max} ?

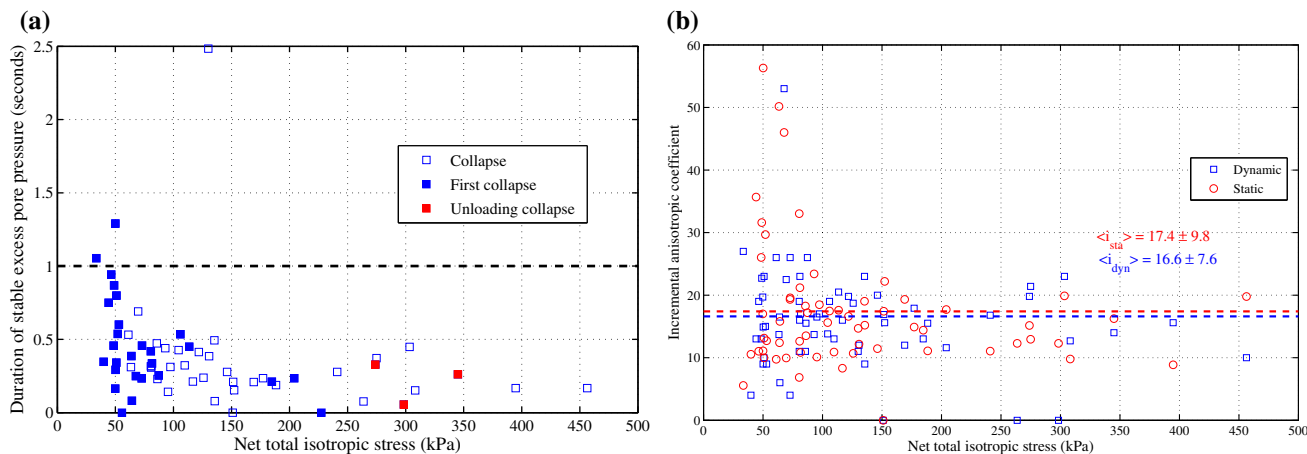


Fig. 10 **a** Effects of net total isotropic stress on the duration of stabilized excess pore pressure for isotropic collapses in compression (blue squares), including unloading collapse (red symbols) and first collapse (solid squares). **b** and on the static i_{sta} and dynamic i_{dyn} incremental anisotropic coefficient (colour figure online)

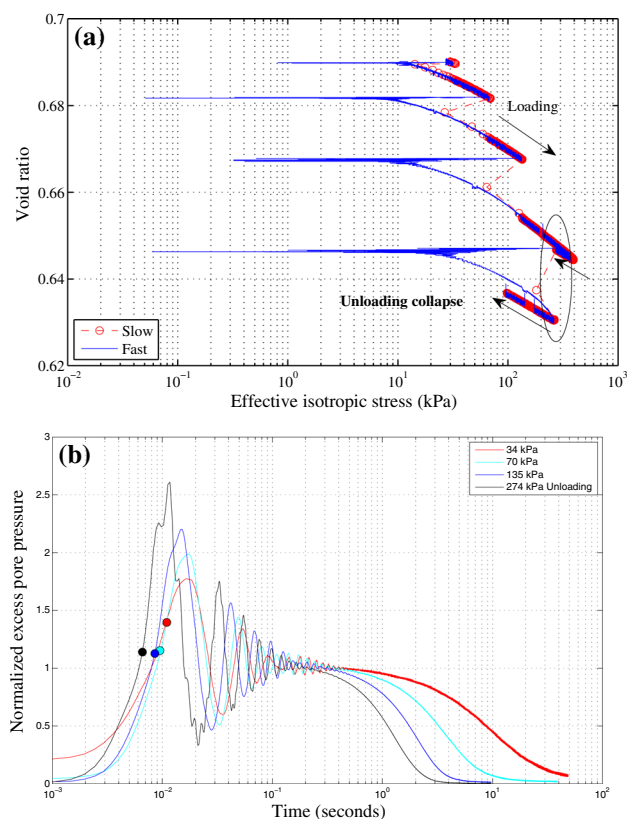


Fig. 11 Effects of void ratio on isotropic collapses and on pore pressure evolution of test overconsolidated test S1 ($e_{30} = 0.690$)

Figure 11a gives the first and rare event of a collapse observed at $\sigma'_{trig} = 274$ kPa during the unloading part from $\sigma'_{max} = 400$ kPa down to 100 kPa of an overconsolidated test S1 with $e_{30} = 0.690$ and $OCR = 4$. While the three collapses in loading are expected for this loose sample, this

sudden collapse in unloading (hollow ellipse) is totally unexpected within the presumably quasi-elastic and stable region. Furthermore it creates a single largest void ratio reduction $\Delta e = 0.016$ of this test; and is even relatively larger than the largest void ratio reduction $\Delta e = 0.013$ of the third collapse event at $\sigma'_{trig} = 135$ kPa during the isotropic loading path; thus, obliterating the small volumetric dilation $\Delta e = 0.0023$ obtained from the unloading part beginning at σ'_{max} . Past this unforeseen collapse in unloading, the sample resumes its normal unloading behaviour with slope $C_s \approx C_c$ towards the final consolidation stress of 100 kPa.

Figure 11b indicates a more violent and narrow peak $\Delta U_{max}^{norm} = 2.61$, a faster dominant vibration frequency and shorter dissipation characteristics for the unloading collapse (shortest t_{50} , shortest dissipation time and largest slope C).

4.5 Collapse in isotropic cycles

Another question emerges following the stunning existence of the first unloading collapse: Can these sudden collapses appear in subsequent drained isotropic compression cycles?

Figure 12a indicates the lack of collapses in a set of 8 isotropic cycles between 20 and 500 kPa on a medium sample of test S5 with $e_{20} = 0.654$ ($Dr = 28.6\%$), excepting the usual collapses during virgin loading. It means a relative stable and resilient granular structure below $\sigma'_{max} = 500$ kPa. The first and only quintuple collapse shows the existence of multiple after-collapses within the largest collapse of $\Delta e = 0.0203$ at 169 kPa of this study. This fact suggests the rapid successive rearrangements of granular structure. Without the after-collapses, the extrapolations

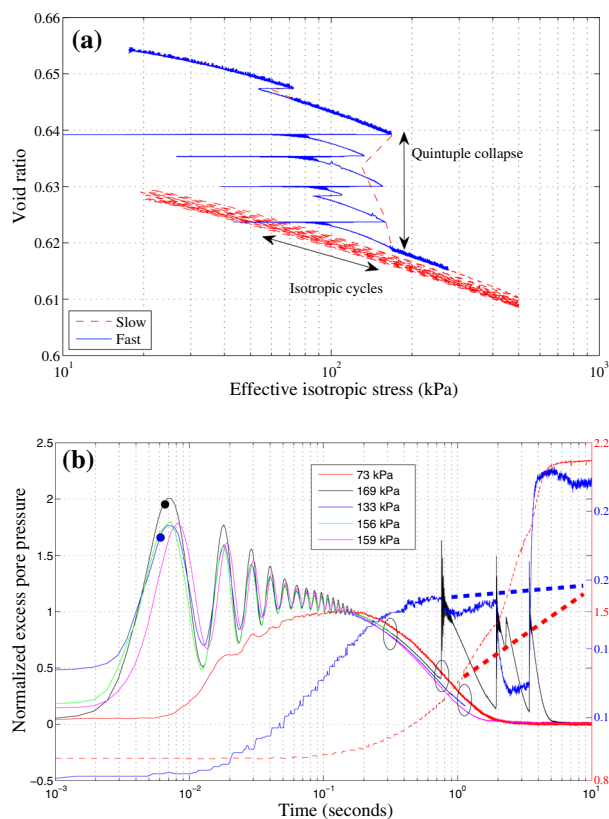


Fig. 12 **a** Quintuple collapse at 169 kPa of test S5, $e_{20} = 0.654$ ($D_r = 28.6\%$). **b** Normalized behaviour of pore water pressure, axial strain and volumetric strain for quintuple collapse (colour figure online)

(dashed thick lines) give only half of $\Delta\varepsilon_v$ and $\Delta\varepsilon_a$ for a single collapse.

As in Sect. 3.2, the development of $\Delta U_{\max}^{\text{norm}}$ for successive collapses in Fig. 12b has all the characteristics; particularly the vibrationless during the transient phase of the first collapse at 73 kPa and the lack of liquefaction for denser state. The last after-collapse at 159 kPa modifies substantially in increasing ε_v and in a complicated pattern for ε_a , including an axial extension jump for the second after-collapse at 156 kPa, contrary to the observations on the triple collapse in Fig. 5. At present state, it is difficult to devise a mechanism for this rare quintuple collapse in cascade.

As expected from granular mechanics, the small hysteretic loops of unload-reload cycle with red colour in Fig. 12a give an accumulated ongoing compaction. Each unload and reload segment is approximately linear.

However, Fig. 13a shows the compressibility behaviour of 5 cycles from 30 to 500 kPa of test S6 on a looser sample with $e_{30} = 0.707$ and a unique collapse (ellipse) appears on the unloading part of the second cycle at 345 kPa. Subsequent isotropic cycles reconfirm the quasi-reversibility of model granular material with $C_s \approx C_c$ with no additional collapse. The corresponding ε_a and ε_v are shown in Fig. 13b measuring an exceptionally larger

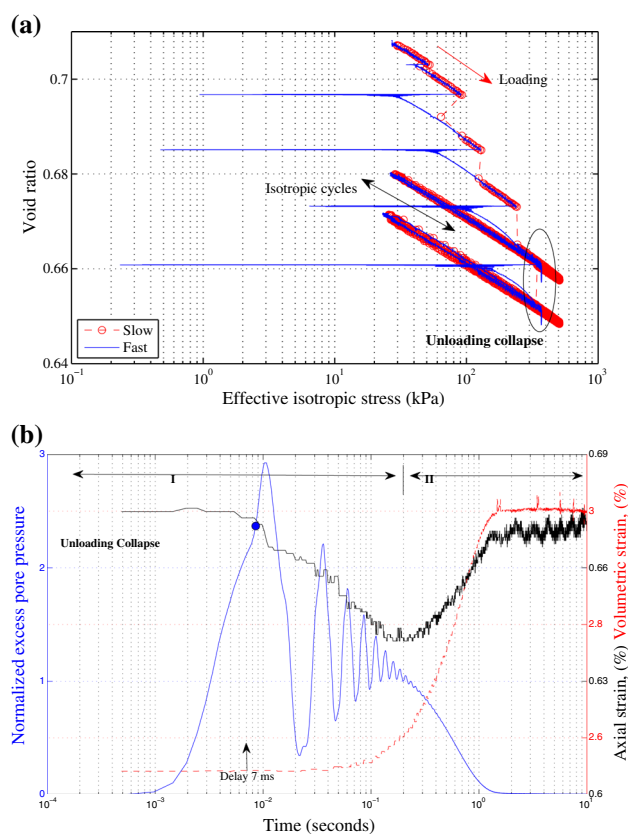


Fig. 13 **a** Spontaneous unloading collapses on third isotropic unloading path at 345 kPa of test S6, $e_{30} = 0.707$ ($D_r = -12.9\%$). **b** Normalized behaviour of pore water pressure, axial strain and volumetric strain for unloading collapse

$\Delta U_{\max}^{\text{norm}} = 2.9$ together with an unusual small axial extension and an always volumetric compaction.

While these two unloading collapses constitute the only two rare events observed during the whole overconsolidated and cyclic test series, they suggest the existence of a new instability behaviour, always associated with a volumetric compaction, clearly within the established stable domain below VCL. It means the metastable microstructure obtained up to σ'_{\max} remains unstable, and it can experience additional collapse at any time for any stress level below σ'_{\max} . The rarity of unloading collapse suggests the still metastability of the obtained microstructure. It paves the way for the possible existence of stick–slip phenomenon in unloading for triaxial compression, which was never been observed before in experiments, and also in triaxial extension, which was never been performed in the laboratory.

4.6 Stick–slip in isotropic consolidation versus drained triaxial compression

Numerous questions raised by previous works on the stick–slip phenomenon in drained compression, [16], concern the

sudden, unexpected ΔU development and ε_v , ε_a jumps during slip phase: How to explain the existence of short-lived excess pore pressure in drained compression? Do the samples experience simultaneously instantaneous axial contraction and volumetric compaction during slip phase?

Figure 14 shows the subsequent stick–slip experience in triaxial drained compression under 500 kPa of test N4. As a comparison with previous isotropic collapses, we focus on the first stick–slip (hollow circle) with largest jump in ε_a and ε_v ; and Fig. 14b gives the time evolution of ΔU , ε_v , ε_a and deviatoric stress $q = \sigma'_a - \sigma'_r$ of this first slip; σ'_a and σ'_r being the effective axial and radial stresses. With the exception of sudden deviatoric stress drop Δq to zero in less than 2 ms due to the presence of deviatoric stress shearing, the evolutionary characteristics of ΔU , ε_v and ε_a of slip phase are qualitatively similar to those of spontaneous collapse under isotropic consolidation as in Fig. 5, since shortly after the end of the slip phase, the persisting vanished q gives an almost effective isotropic stress state for the rest of slip phase. The inferred liquefaction level (solid red circle), just above the unit normalized level, indicates a vanishing σ'_r for almost 200 ms or a local liquefaction state.

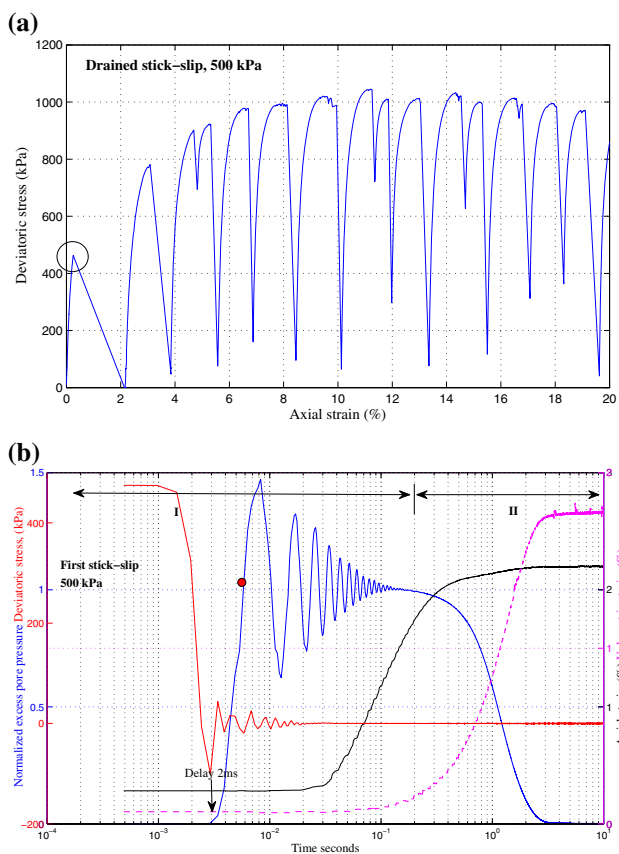


Fig. 14 Stick–slip phenomenon in drained triaxial compression at constant confining pressure of 500 kPa of test N4, $e_{30} = 0.688$, $e_c = 0.665$ ($Dr = 19.1\%$): **a** stress–strain behaviour, **b** slip phase of first stick–slip

The slip phase in compression stick–slip experiments is characterized by a very fast deviatoric stress drop, an equally fast transient phase of ΔU followed by a comparable dissipation period with $t_{50} = 1.12$ s, a delayed and progressive evolution of ε_a and ε_v as σ'_r recovers to the previous level before slip. Subsequent stick–slips have similar behaviour and an in-depth time-resolved study of stick–slip phenomenon will be published elsewhere.

While this paper cannot offer a logical explanation for the unpredictable ΔU , it gives nevertheless some new insights into the dynamic behaviour during slip phase, solving then at least some small mysteries of stick–slip phenomenon occurring in model granular media (instantaneous deviatoric stress drop, local liquefaction state and progressive evolution of ε_a and ε_v). The systematic observed small delay of ΔU development with respect to Δq for all stick–slips as in Fig. 14b excludes logically ΔU as the first cause of slip instability. The brevity of Δq points to the possible failure of contact force chains, and ΔU as a consequence thereof. Rapid pore pressure generation was also measured in thin shear zones shortly after the initiation of flowslides on loose coking coal [22]. Nevertheless, the interstitial pore pressure still plays a major role in the amplification of these instabilities in fully saturated media in reducing the effective stress.

In the literature, the incompleteness of the observed ε_a and ε_v and even ΔU jumps in stick–slip experiments is due only to the inadequate characteristics of the data acquisition system for a dynamic phenomenon, [2, 5, 9, 16, 78].

4.7 Structural instability hypothesis

To verify the role of pore fluid pressure, some complementary tests were performed on unsaturated moist and on dry and medium dense samples in Fig. 15. The transient phase I is still measured; however, without oscillations with small pore pressure development up to $\Delta U_{stable} = 9.6$ kPa. Consequently, the fluid pressure is not the initial cause for the observed isotropic instabilities in this study, as in shear stick–slip experiments in the literature [2, 32, 48], or in triaxial compression shear on dry sand with diffuse failure [64].

One possible speculated explanation is that these events resulted from structural instability of metastable microstructure along preferential force chains carrying most of the applied stress within the granular assembly [21, 40, 77]. The sudden breakage or buckling of these chains, facilitated by the rolling feature of perfect spherical grain shape, noticed in numerical experiments [74], can induce local dynamic shear deformation, and result in a fast pore water pressure buildup due to the incompressibility of water in a fully saturated media. The temporary decrease in effective stress would, in turn, promote further

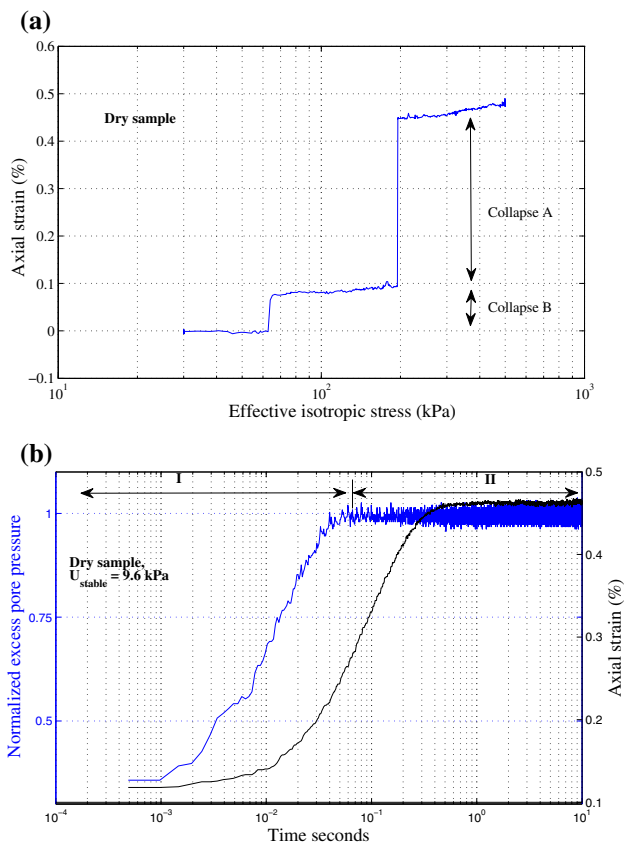


Fig. 15 Dynamic dry collapses at 62 and 197 kPa of medium dense specimen: **a** compressibility behaviour. **b** Normalized behaviour of pore water pressure and axial strain for the largest collapse

deformation, and help in explaining the larger magnitude of collapses in saturated shear experiments, compared to dry ones. The spontaneity of slip events in experiments [26, 48, 49, 72], of less than 2 ms in case of shear stick-slip, can be seen in Fig. 14.

The sudden release of accumulated energy and the subsequent rapid micro-structural rearrangement might generate some elastic waves [4, 39], and extend a step further the conjecture of dynamic pore pressure fluctuations formulated earlier in rapid shearing experiments [33]. The oscillating underdamped feature of ΔU during transient phase in Fig. 9a is the first experimental evidence to support these hypotheses. The strong connection between the slip event during shear and the low frequency acoustic emission in annular shear tests [47], although without clear experimental correlation, and the systematic audible sound accompanied isotropic collapses in this paper, could point to the physical origin of these instabilities within granular mass [46]. The sudden breakage of the force chains can make two adjoining grains vibrate during the breakage event and then produce the audible frictional sound [20, 53].

The notoriously difficult experimental micromechanical investigation can get some insights from discrete element modelling (DEM) technique. The collapse of force chains is strongly correlated to stress drops in slip phase on biaxial test simulations using a packing of polygonal particles [54]; or on triaxial tests with spherical ones [70]. The role of pore fluid is of paramount importance in recent advanced studies on a nearly monodispersed population of spherical grains, with a full solid-liquid coupling formulation [27, 28]. Drained triaxial compression can briefly experience multiple localized liquefaction states. Unfortunately, the triggering mechanisms and the dynamic characteristics of pore pressure evolution are still missing in these numerical experiments. The lack of direct observations, a still challenging task despite the availability of modern μ -tomography technique, [13, 31] and advanced two or three-dimensional imaging techniques using epoxy impregnation, [25], leaves these enigmatic aspects unsolved.

This structural instability hypothesis can help to explain qualitatively the existence of successive collapses in a short time period. As force network recovers from previous breakdown, some newly rebuilt force chains can have insufficient strength to support the actual stress, and sudden breakage of these chains can happen before getting full strength.

The leading candidates for the observed dynamic instabilities are the rolling resistance [23, 74] and the contact ageing [32, 69] of spherical particles along force columns. If this is not the answer, the possible explanations become strange, such as mysterious observed “doublets” or solid bridges [16] in stick-slip experiments that can break, or the stochastically determined failure of fibre bundle model [30]; and if all else fails, there is a chance some ingredients are missing with our basic understanding of micromechanical friction laws. In our knowledge, these dynamic isotropic instabilities, as well as stick-slip shear ones with strong volumetric coupling, were never been observed before in numerical studies, nor theoretically predicted.

4.8 Collapse-free void ratio

Can we identify a collapsed fabric void ratio e_{30}^{col} , representing the transition from local instability with partial liquefaction to collapse-free during isotropic consolidation? Fig. 16a shows the compressibility behaviour on an isotropic cycle from 30 to 400 kPa of a dense sample created by dry deposition technique with $e_{30} = 0.596$ ($Dr = 80.3\%$).

A nearly smooth and collapse-free behaviour is obtained. However, close examination reveals three tiny collapses A to C in loading at 64, 136, 264 kPa and one unloading collapse D at 298 kPa. The largest collapse A

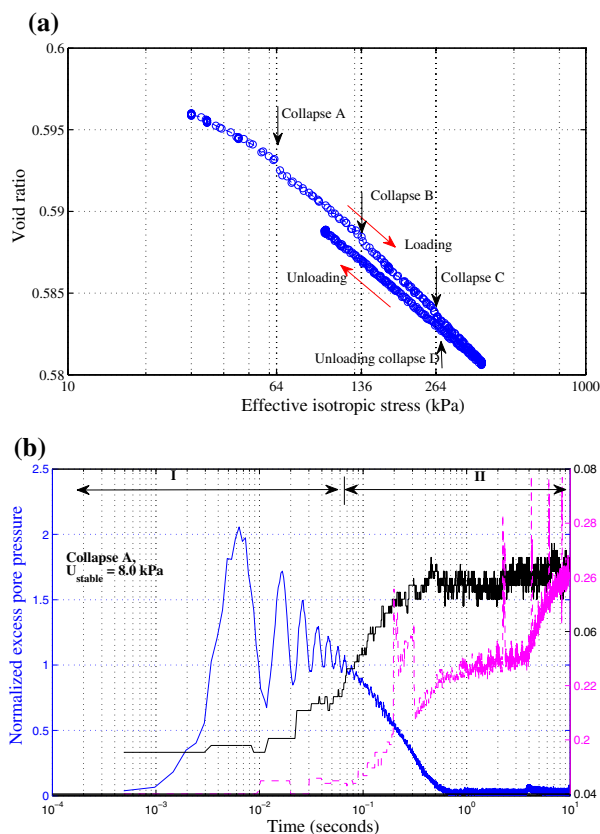


Fig. 16 Isotropic consolidation of dense sample $e_{30} = 0.596$ ($Dr = 80.3\%$) created by dry deposition method of test SP1. **a** Compressibility behaviour with a rare unloading collapse D at 298 kPa. **b** Normalized behaviour of pore water pressure, axial strain and volumetric strain for largest collapse A at 64 kPa

has a discernible Δe of about only 0.001, and a small $\Delta U_{stable} = 8.0$ kPa, the same order of magnitude of moist sample, with a transient phase *I* reasonably delineated in Fig. 16b and a shortest $t_{50} = 0.218$ s in the dissipation phase *II*. The remaining collapses are macroscopically indiscernible.

A complete collapse-free behaviour during some isotropic cycles is obtained on a more denser sample with $e_{30} = 0.584$ ($Dr = 91.1\%$) of test SP2.

Some additional observations can be made from these special tests. First, the threshold collapsed fabric void ratio e_{30}^{col} can be approximated to 0.590 ($Dr = 85.7\%$) with a total disappearance of collapses for denser samples below this value in Fig. 17. The second is small collapses above e_{30}^{col} , including the unloading accidents, have no practical consequences on the global compressibility behaviour. The existence of collapse unloading, although rare, constitutes the third observation. The fourth points to the collapses for dense body; it can convey an explanation for the shear stick–slip behaviour happening in high density and at the steady-state of an initially loose sample [16]. The final and

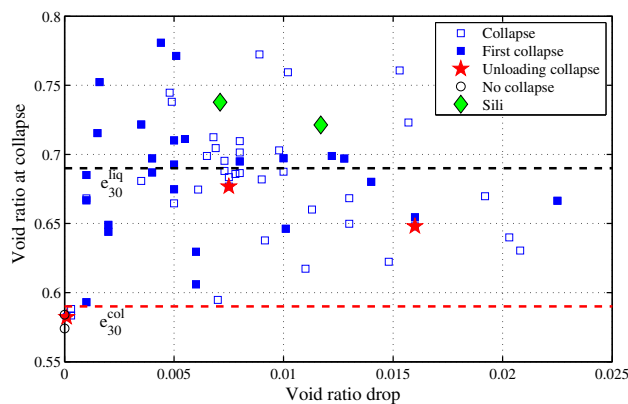


Fig. 17 Identification of threshold void ratio e_{30}^{col} indicating a total disappearance of dynamic collapses on dense samples (colour figure online)

major observation concerns the occurrence of collapses for all tested samples in this study, irrespective of initial density and depositional methods. Consequently, this collapsibility seems to be an inherent characteristic driven by e_{30} .

Figure 17 collects Δe and e_{trig} , the void ratio at σ'_{trig} , for all collapses and a threshold void ratio e_{30}^{col} can be reasonably identified. It can be one physical attribute controlling the disappearance of collapses on dense samples. The first collapse (full symbols) has usually smaller Δe than the subsequent or unloading collapses. Logically e_{30}^{col} is lower than the previously identified liquefaction-free threshold $e_{30}^{liq} = 0.690$ ($Dr = -11.6\%$) for the same materials [19]. Coincidentally, $e_{30}^{col} \approx e_{min}$ and $e_{30}^{liq} \approx e_{max}$, the two normative values defining the usable range of void ratio.

Can these dynamic collapses happen for other glass beads? Tests with CVP smaller beads of 0.4 mm indicate that collapses still occur and excess pore pressure persists to experience the basic 2-phase response features as other reported collapses but accompanies by some distinctions (low frequency, longer duration for the whole dynamical response in collapse ...). Furthermore, Fig. 18a shows the compressibility from 30 to 500 kPa of soda-lime “Sili-beads” type S, well-sorted and well rounded with similar $D_{50} = 0.675$ mm, commercialized by sigmund-lindner, Germany². As expected, loose sample with $e_{30} = 0.750$ experiences two large collapses at 146 and 400 kPa. The results are broadly consistent with previous observations on CVP beads. The ΔU^{norm} , $\Delta \epsilon_v$ and $\Delta \epsilon_a$ for the second collapse, shown in Fig. 18b, strengthen the collapsibility of soda-lime glass beads, with some variations (fewer oscillations, smaller frequency, highly damped system). These

² www.sigmund-lindner.com.

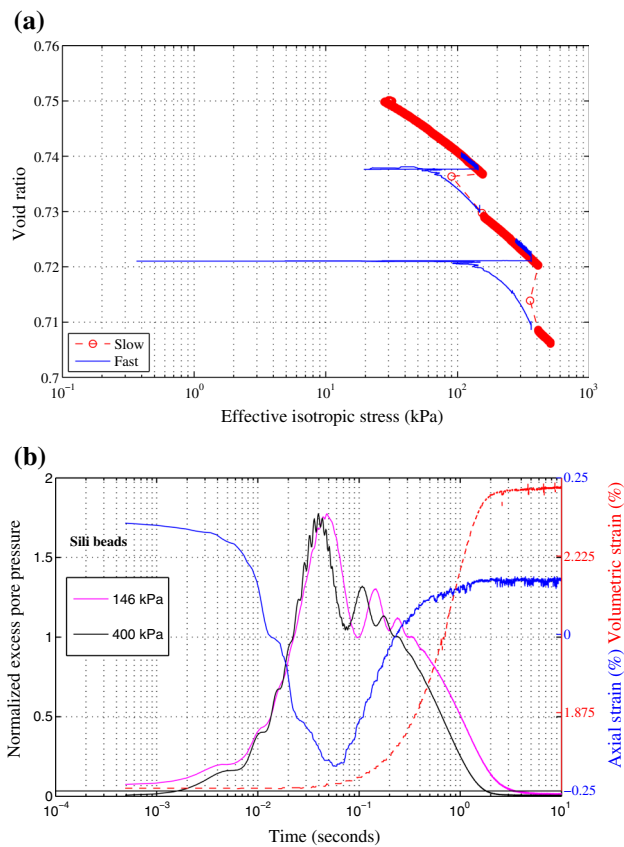


Fig. 18 Isotropic consolidation of Silibeads sample with $e_{30} = 0.750$. **a** Compressibility behaviour. **b** Normalized behaviour of pore water pressure, axial strain and volumetric strain for largest collapse B at 400 kPa

differences can be attributed to different industrial fabrication processes. Future studies will address a complete comparison.

5 Conclusions

The compressibility behaviour of fully water-saturated monodisperse glass beads, normally consolidated and overconsolidated, initially assembled in loose state by moist-tamping technique, under **isotropic drained** compression, is affected by unexpected events triggered at undetermined effective isotropic stress. In compression loading, as well as in unloading, each event is characterized by two phases. The first dynamic transient phase *I* has a very fast drop of effective isotropic stress σ' due to an excess pore pressure development ΔU at nearly constant volume and constant axial strain. ΔU vibrates like an oscillating underdamped system and briefly creates a local liquefaction state with null σ' . The second quasi-static phase *II* follows with gradual increase in axial ε_a (contraction) and volumetric ε_v (compaction) strain, and a full

progressive recovery of σ' to the previous steady-state level before event. These events closely resemble the stick–slip instability during shear in triaxial drained compression. Rare collapse events even occur during the isotropic unloading, always under undetermined σ' . These unloading collapses share the same characteristics as those of loading. Instability also happens for unsaturated moist and dry states. Upon ignoring these stick–slip events, the classical compressibility behaviour of granular material is recovered having a quasi-elastic behaviour with $C_s \approx C_c$. The stick–slip-like phenomenon tends to increase asymptotically in amplitude of volumetric strain at greater isotropic stress towards a constant value, while keeping small axial strain. A same kinematic strain development for both quasi-static and dynamic phases is observed.

The isotropic triaxial consolidation is collapse-free for dense state below a threshold void ratio at 30 kPa of confining pressure, e_{30}^{col} , representing the transition from local instability with partial liquefaction to smooth compressibility behaviour. This threshold e_{30}^{col} completes nicely with previously identified liquefaction-free threshold e_{30}^{liq} . Together, they define the void ratio range for dynamic instabilities. The revealed collapsibility, irrespective of initial density and depositional methods, is an essential feature, and can be an important clue to the physical cause beneath the strange observed instabilities.

It is suspected that two ingredients are required to create these isotropic dynamic collapses: an initial highly structural anisotropic state and the spherical form of particles. An additional requirement for lower density above a threshold e_{30}^{liq} is also expected for a full isotropic liquefaction.

It is also **hypothesized** that unforeseen large dynamic pore pressure fluctuations can be originated in micro-structural instability resulting from local collapse of contact networks and subsequent rapid micro-structural rearrangements. Consequently, the pore fluid is not the cause of these events. It is responsible only for the amplification of the event, since large pore pressure fluctuations can reduce significantly the effective isotropic stress, decrease in turn the grain-contact stresses towards a vanishing stress state and increase the axial and volumetric strain. Isotropic instabilities and shear stick–slips share probably the same physical origin with strong links to geometrical features.

Some obvious questions remain: Can these dynamic instabilities appear in polydispersed model granular materials? What are the necessary conditions to initiate, propagate and maintain these short-lived local collapses? How these local events can sustain long enough, for more than one second, to create a global liquefaction state with large deformation and catastrophic consequences? However, the main critical and long-standing question to be answered is

what are the cause or combination of causes of this large pore pressure buildup, in other words what are the physical triggering mechanisms responsible for the creation of these events? No satisfactory explanations have yet emerged from scientific studies. More experimental and numerical works are needed to address these issues.

Since special care was taken in double measuring and checking the dynamic pore fluid pressure, some more unanswered questions persist: What are the physical information encoded in the transient phase? Can we derive some dynamic material characteristics?

There is a strong possibility that the inexplicable observed dynamic instabilities may have been a permanent phenomenon rather than a brief historical anomaly of idealized granular behaviour. Based on these surprising experimental findings, the ideal perfectly spherical particles, especially glass beads, can hardly be substituted for real granular materials.

The test data of this paper can be downloaded from the journal website as supplementary materials.

Acknowledgements The authors would like to thank J. Scheibert and J.-N. Roux, for very fruitful discussions; C. Dano for providing e_{\min} , e_{\max} and the SEM figures; J. Blanc-Gonnet, S. Cointet, L. Giraud, M. Guibert, D. Roux, F. Sallet and S. Zara for technical supports; and two anonymous reviewers for helpful suggestions making this work synthetic and attractive.

References

- Adjemian F (2003) Stick–slip et transition de brouillage dans les essais triaxiaux sur billes de verre. Thèse de doctorat, Ecole Centrale Paris
- Adjemian F, Evesque P (2004) Experimental study of stick–slip behaviour. *Int J Numer Anal Methods Geomech* 28(6):501–530
- Agnolin I, Roux J-N (2007) Internal states of model isotropic granular packings. II. Compression and pressure cycles. *Phys Rev E* 76(6):061303
- Aharonov E, Sparks D (2004) Stick-slip motion in simulated granular layers. *J Geophys Res* 109:B09306
- Alshibli KA, Roussel LE (2006) Experimental investigation of stick–slip behaviour in granular materials. *Int J Numer Anal Methods Geomech* 30(14):1391–1407
- Anthony JL, Marone C (2005) Influence of particle characteristics on granular friction. *J Geophys Res* 110:B08409
- Behringer RP, Howell D, Veje C (1999) Stress fluctuations in a 2D granular Couette experiment: a continuous transition. *Phys Rev Lett* 82(26):5241–5244
- Bjerrum L, Krimstad S, Kummeneje O (1961) The shear strength of a fine sand. In: *Proceedings of 5th international conference on soil mechanics and foundation engineering*, vol 1, pp 29–37
- Çabalar AF, Clayton CRI (2010) Some observations of the effects of pore fluids on the triaxial behaviour of a sand. *Granul Matter* 12(1):87–95
- Cain R, Page N, Biggs S (2001) Microscopic and macroscopic aspects of stick–slip motion in granular shear. *Phys Rev E* 64(1):0164131–8
- Cundall PA, Strack ODL (1979) A discrete numerical model for granular assemblies. *Géotechnique* 29(1):47–65
- Daouadji A, Darve F, Al Gali H, Hicher PY, Laouafa F, Lignon S, Nicot F, Nova R, Pinheiro M, Prunier F, Sibille L, Wan R (2011) Diffuse failure in geomaterials: experiments, theory and modelling. *Int J Numer Anal Methods Geomech* 35(16):1731–1773
- Desrues J, Chambon R, Mokni M, Mazerolle F (1996) Void ratio evolution inside shear bands in triaxial sand specimens studied by computed tomography. *Géotechnique* 46(3):527–546
- Dieterich JH (1979) Modeling of rock friction I. Experimental results and constitutive equations. *J Geophys Res* 84(B5):2161–2168
- Doanh T, Abdelmoula N, Nguyễn TTT, Hans S, Boutin C, Le Bot A (2016) Unexpected liquefaction under isotropic consolidation of idealized granular materials. *Granul Matter* 18(3):67
- Doanh T, Hoang MT, Roux J-N, Dequeker C (2013) Stick–slip behaviour of model granular materials in drained triaxial compression. *Granul Matter* 15(1):1–23
- Doanh T, Ibraim E (2000) Minimum undrained strength of Hostun RF. *Géotechnique* 50(4):377–392
- Doanh T, Le Bot A, Abdelmoula N, Gribaa L, Hans S, Boutin C (2016) Unexpected collapses during isotropic consolidation of model granular materials. *Comptes Rendus Mécanique* 344(2):66–77
- Doanh T, Le Bot A, Abdelmoula N, Hans S, Boutin C (2014) Liquefaction of immersed granular media under isotropic compression. *Europhys Lett* 108(2):24004
- Donescu S, Munteanu L, Mosneguțu V (2011) On the acoustics of the stick–slip phenomenon. *Rev Roum Sci Tech Méc Appl* 56(2):105–111
- Drescher A, de Jong G De Josselin (1972) Photoelastic verification of a mechanical model for the flow of a granular material. *J Mech Phys Solids* 20:337–351
- Eckersley D (1990) Instrumented laboratory flowslides. *Géotechnique* 40(3):489–502
- Estrada N, Taboada A, Radjai F (2008) Shear strength and force transmission in granular media with rolling resistance. *Phys Rev E* 78:021301
- Finge Z, Doanh T, Dubujet Ph (2006) Undrained anisotropy of Hostun RF loose sand: new experimental hints. *Can Geotech J* 43(11):1195–1212
- Frost JD, Jang DJ (2000) Evolution of sand microstructure during shear. *J Geotech Geoenviron Eng* 126(2):116–130
- Géminard JC, Losert W, Gollub JP (1999) Frictional mechanics of wet granular material. *Phys Rev E* 59(5):5881–5890
- Goren L, Aharonov E, Sparks D, Toussaint R (2010) Pore pressure evolution in deforming granular material: a general formulation and the infinitely stiff approximation. *J Geophys Res* 115:B09216
- Goren L, Aharonov E, Sparks D, Toussaint R (2011) The mechanical coupling of fluid-filled granular material under shear. *Pure Appl Geophys* 168(12):2289–2323
- Gudehus G (2010) *Physical soil mechanics*. Springer, Berlin
- Halasz Z, Kun F (2009) Fiber bundle model with stick–slip dynamics. *Phys Rev E* 80(2):027,102
- Hall SA, Bornert M, Desrues J, Pannier Y, Lenoir N, Viggiani G, Bésuelle P (2010) Discrete and continuum analysis of localised deformation in sand using X-ray μ CT and volumetric digital image correlation. *Géotechnique* 60(5):315–322
- Heslot F, Baumberger T, Perrin B, Caroli B, Caroli C (1994) Creep, stick–slip, and dry-friction dynamics: experiments and a heuristic model. *Phys Rev E* 49(6):4973–4988
- Iverson RM, LaHusen RG (1989) Dynamic pore-pressure fluctuations in rapidly shearing granular materials. *Science* 246(4931):796–799

34. Kim MS (1995) Etude expérimentale du comportement mécanique des matériaux granulaires sous forte contrainte. Thèse de doctorat, Ecole Centrale Paris
35. Kumar N, Luding S (2016) Memory of jamming—multiscale flow in soft and granular matter. *Granul Matter* 18(3):58
36. Ladd RS (1978) Preparing test specimens using undercompaction. *Geotech Test J* 1(1):16–23
37. Lade PV, Duncan JM (1973) Cubical triaxial tests on cohesionless soil. *J Soil Mech Found ASCE* 99(10):793–812
38. Lagioia R, Nova R (1995) An experimental and theoretical study of the behaviour of a calcarenite in triaxial compression. *Géotechnique* 45(4):633–648
39. Liu CH, Nagel SR (1993) Sound in a granular material: disorder and nonlinearity. *Phys Rev B* 48(21):15,646–15,650
40. Liu CH, Nagel SR, Schecter DA, Coppersmith SN, Majmudar S (1995) Force fluctuations in bead packs. *Science* 269(5223):513–515
41. Mair K, Frye KM, Marone C (2002) Influence of grain characteristics on the friction of granular shear zones. *J Geophys Res* 107(B10):2219
42. Marone C (1998) Laboratory-derived friction laws and their application to seismic faulting. *Annu Rev Earth Planet Sci* 26:643–696
43. Mašin D (2012) Asymptotic behaviour of granular materials. *Granul Matter* 14(6):759–774
44. McDowell GR, de Bono JP (2013) On the micro mechanics of one-dimensional normal compression. *Géotechnique* 63(11):895–908
45. McDowell GR, De Bono JP, Yue P, Yu H-S (2013) Micro mechanics of isotropic normal compression. *Géotech Lett* 3(4):166–172
46. Michlmayr G, Cohen D, Or D (2012) Sources and characteristics of acoustic emissions from mechanically stressed geologic granular media—a review. *Earth Sci Rev* 112(3):97–114
47. Michlmayr G, Or D (2014) Mechanisms for acoustic emissions generation during granular shearing. *Granul Matter* 16(5):627–640
48. Nasuno S, Kudrolli A, Bak A, Gollub JP (1998) Time-resolved studies of stick–slip friction in sheared granular layers. *Phys Rev E* 58(2):2161–2171
49. Nasuno S, Kudrolli A, Gollub JP (1997) Friction in granular layers: hysteresis and precursors. *Phys Rev Lett* 79(5):949–952
50. Oda M, Iwashita K (1999) *Mechanics of granular materials: an introduction*. CRC Press, Boca Raton
51. O’Sullivan C (2011) *Particulate discrete element modelling*. Spon Press, Boca Raton
52. O’Sullivan C, Cui L (2009) Micromechanics of granular material response during load reversals: combined DEM and experimental study. *Powder Technol* 193(3):289–302
53. Patitsas AJ (2010) Squeal vibrations, glass sounds, and the stick–slip effect. *Can J Phys* 88(11):863–876
54. Peña AA, Lizcano A, Alonso-Marroquin F, Herrmann HJ (2008) Biaxial test simulations using a packing of polygonal particles. *Int J Numer Anal Methods Geomech* 32(2):143–160
55. Persson BNJ (1998) *Sliding friction*. Springer, Berlin
56. Radjai F, Roux S (2004) Contact dynamics study of 2D granular media: critical states and relevant internal variables. In: Hinrichsen H, Wolf DE (eds) *The physics of granular media*. Wiley-VCH, Berlin, pp 165–187
57. Radjai F, Dubois F (2011) *Discrete numerical modeling of granular materials*. Wiley, New York
58. Radjai F, Evesque P, Bideau D, Roux S (1995) Stick-slip dynamics of a one-dimensional array of particles. *Phys Rev E* 52(5):5555–5564
59. Ramos AM, Andrade JE, Lizcano A (2012) Modelling diffuse instabilities in sands under drained conditions. *Géotechnique* 62(4):471–478
60. Roussel LE (2003) *Experimental investigation of stick-slip behaviour in granular materials*. Louisiana State University, Master of science in civil engineering
61. Ruina A (1983) Slip instability and state variable friction law. *J Geophys Res* 88(B12):10,359–10,370
62. Sitharam TG, Vinod JS (2009) Critical state behaviour of granular materials from isotropic and rebounded paths: DEM simulations. *Granul Matter* 11(1):33–42
63. Skempton AW, Taylor RN (1954) The pore pressure coefficients A and B. *Géotechnique* 4(4):143–147
64. Skopek P, Morgenstern NR, Robertson PK, Sego DC (1994) Collapse of dry sand. *Can Geotech J* 31(6):1008–1014
65. Suiker ASJ, Fleck NA (2004) Frictional collapse of granular assemblies. *ASME J Appl Mech* 71:350–358
66. Terzaghi K, Peck RP, Mesri G (1996) *Soil mechanics in engineering practice*, 3rd edn. Wiley, New York
67. Thompson P, Grest G (1991) Granular flow: friction and dilatancy transition. *Phys Rev Lett* 67(13):1751–1754
68. Thornton C (2000) Numerical simulations of deviatoric shear deformation of granular media. *Géotechnique* 50(1):43–53
69. Tong L, DEM Wang YH (2015) Simulations of shear modulus and damping ratio of sand with emphasis on the effects of particle number, particle shape, and aging. *Acta Geotech* 10(1):117–130
70. Tordesillas A, Hilton JE, Tobin ST (2014) Stick–slip and force chain evolution in a granular bed in response to a grain intruder. *Phys Rev E* 89:042207
71. Trivedi A, Sud VK (2004) Collapse behavior of coal ash. *J Geotech Geoenviron Eng* 130(4):403–415
72. Tsai J-C, Voth GA, Gollub JP (2003) Internal granular dynamics, shear-induced crystallization, and compaction steps. *Phys Rev Lett* 91(6):064301
73. Verdugo R, Ishihara K (1996) The steady state of sandy soils. *Soils Found* 36(2):81–91
74. Wenzl J, Seto R, Roth M, Butt H-J, Auernhammer GK (2013) Measurement of rotation of individual spherical particles in cohesive granulates. *Granul Matter* 15(4):391–400
75. Wood DM (1990) *Soil behaviour and critical state soil mechanics*. Cambridge University Press, Cambridge
76. Wood DM (1994) General report: evaluation of material properties. In: Miura S, Shibuya S, Mitachi T (eds) *Proceedings of pre-failure deformation of geomaterials, Sapporo, Japan, vol 2, Balkema, Rotterdam*, pp 1179–1199
77. Wood DM, Lesniewska D (2011) Stresses in granular materials. *Granul Matter* 13(4):395–415
78. Yang J, Wei LM (2012) Collapse of loose sand with the addition of fines: the role of particle shape. *Géotechnique* 62(12):1111–1125